Atmospheric Environment 320 (2024) 120325

Contents lists available at ScienceDirect

Atmospheric Environment

journal homepage: www.elsevier.com/locate/atmosenv

Estimation of ammonia deposition to forest ecosystems in Scotland and Sri Lanka using wind-controlled NH_3 enhancement experiments

Ajinkya G. Deshpande [a,*], Matthew R. Jones [a], Netty van Dijk [a], Neil J. Mullinger [a], Duncan Harvey [a], Robert Nicoll [a], Galina Toteva [a,b], Gothamie Weerakoon [c], Sarath Nissanka [d], Buddhika Weerakoon [d], Maude Grenier [a], Agata Iwanicka [a], Fred Duarte [a], Amy Stephens [a], Christopher J. Ellis [e], Massimo Vieno [a], Julia Drewer [a], Pat A. Wolseley [c], Shamodi Nanayakkara [f], Tharindu Prabhashwara [f], William J. Bealey [a], Eiko Nemitz [a], Mark A. Sutton [a]

[a] UK Centre for Ecology and Hydrology, Edinburgh Research Station, Penicuik, EH26 0QB, UK
[b] University of Edinburgh, EH8 9YL, UK
[c] Natural History Museum, London, SW7 5BD, UK
[d] University of Peradeniya, Kandy, 20400, Sri Lanka
[e] Royal Botanic Garden, Edinburgh, EH3 5NZ, UK
[f] Dilmah Conservation, Paliyagoda, 11830, Sri Lanka

HIGHLIGHTS

- Wind-controlled field NH_3 release systems replicate real-world pollution scenarios and are a tool for assessing ecological impacts of NH_3.
- Our resistance model aids quantifying NH_3 deposition to different layers of a forest canopy from an NH_3 source located within the canopy.
- The NH_3 release system coupled with the resistance model shows that soil surface and leaf cuticles experience the highest NH_3 deposition.

GRAPHICAL ABSTRACT

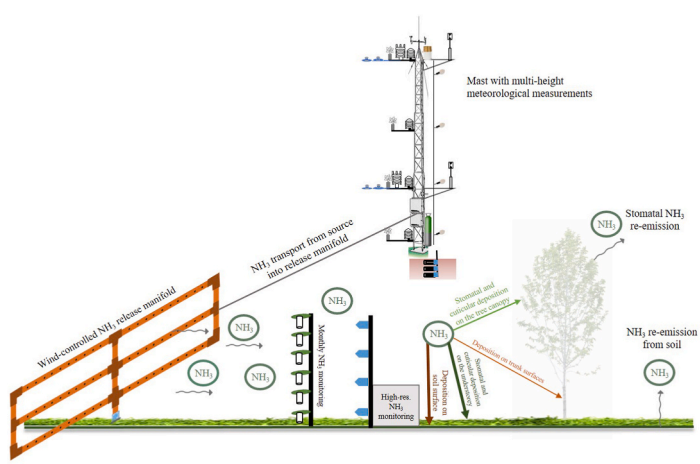

ARTICLE INFO

Keywords:
Ammonia
Dry deposition
Enhancement

ABSTRACT

Ammonia (NH_3) pollution has emerged as a major cause of concern as atmospheric concentrations continue to increase globally. Environmentally damaging NH_3 levels are expected to severely affect sensitive and economically important organisms, but evidence is lacking in many parts of the world. We describe the design and operation of a wind-controlled NH_3 enhancement system to assess effects on forests in two contrasting climates.

* Corresponding author.
E-mail address: ajides@ceh.ac.uk (A.G. Deshpande).

https://doi.org/10.1016/j.atmosenv.2023.120325
Received 25 August 2023; Received in revised form 21 December 2023; Accepted 31 December 2023
Available online 6 January 2024

Field release
Resistance modelling
Compensation point

We established structurally identical NH_3 enhancement systems in a temperate birch woodland in the UK and a tropical sub-montane forest in central Sri Lanka, both simulating real-world NH_3 pollution conditions. Vertical and horizontal NH_3 concentrations were monitored at two different time scales to understand NH_3 transport within the forest canopies. We applied a bi-directional resistance model with four canopy layers to calculate net deposition fluxes. At both sites, NH_3 concentrations and deposition were found to decrease exponentially with distance away from the source, consistent with expectations. Conversely, we found differences in vertical mixing of NH_3 between the two experiments, with more vertically uniform NH_3 concentrations in the dense and multi-layered sub-montane forest canopy in Sri Lanka. Monthly NH_3 concentrations downwind of the source ranged from 3 to 29 μg m^{-3} at the UK site and 2–47 μg m^{-3} at the Sri Lankan site, compared with background values of 0.63 and 0.35 μg m^{-3}, respectively. The total calculated NH_3 dry deposition flux to all the canopy layers along the NH_3 transects ranged from 12 to 162 kg N ha^{-1} yr^{-1} in the UK and 16–426 kg N ha^{-1} yr^{-1} in Sri Lanka, representative of conditions in the vicinity of a range of common NH_3 sources. This multi-layer model is applicable for identifying the fate of NH_3 in forest ecosystems where the gas enters the canopy laterally through the trunk space and exposes the understorey to high NH_3 levels. In both study sites, we found that cuticular deposition was the dominant flux in the vegetation layers, with a smaller contribution from stomatal uptake. The new facilities are now allowing the first ever field comparison of NH_3 impacts on forest ecosystems, with special focus on lichen bio-indicators, which will provide vital evidence to inform NH_3 critical levels and associated nitrogen policy development in South Asia.

1. Introduction

Emissions of gaseous ammonia and its dry deposition are on the rise globally and are projected to increase at least until 2030 (Sutton and Howard, 2018). Although successful attempts have been made to reduce emissions of pollutant compounds like sulphur dioxide (SO_2), nitrogen oxides (NO_x) and aerosol nitrate (NO_3^-) in many parts of the world, NH_3 has proven to be particularly difficult to control (EEA, 2016; Sutton et al., 2020). The UK exemplifies the multifaceted challenge in reducing NH_3, being a region where emissions are on a slow decline (16% from 1998 to 2014) though reduction in atmospheric NH_3 concentration remains insignificant (Tang et al., 2018). Increased emissions from cattle sources have nearly offset the reduced emissions from pig and poultry farming in the UK (Tang et al., 2018), while, rapid reduction in SO_2 emissions and subsequent deceleration of NH_3 neutralization by SO_2 is leading to a longer residence time of NH_3 in the atmosphere (Sutton et al., 2003; Tang et al., 2018). Current mean monthly atmospheric NH_3 concentrations in the UK range from <0.2 to 22 μg m^{-3} (Clean Air Strategy, 2019; Tang et al., 2018) and even higher concentrations are expected near point sources.

As global human population rises and production of food and animal feed is further accelerated, increase in emission of NH_3 is anticipated from associated sources such as fertilizer application, poultry farming, cattle rearing, etc. This acceleration is pronounced in highly populated, developing countries including in South Asia (India, Pakistan, Sri Lanka, Bangladesh and Nepal), which has emerged as having global NH_3 emission and deposition hotspots (Van Damme et al., 2018), especially across the Indo-Gangetic Plain. Ambient concentrations of NH_3 in these areas appear to have crossed toxic levels for sensitive ecosystems such as forests (Ellis et al., 2022).

Significant numbers of rural NH_3 point sources such as pastures, croplands, tea plantations and poultry farms are situated close to or within forests. Moreover, fragmented woodland patches with greater edge effects are especially exposed to such sources. Some tree species are known to have a substantial NH_3 recapture potential (Bealey et al., 2014; Theobald et al., 2001) and show a slower negative response to reactive nitrogen (N_r) deposition (Deshpande, 2020). In contrast, non-vascular plants, fungi and lichens, which provide supporting ecosystem services in forests and woodlands, may not be as resilient as foundational trees and can experience damaging impacts resulting in loss of abundance and decline in species diversity (Cape et al., 2009; Wolseley et al., 2006). Therefore, in forests and woodlands close to ammonia sources, trees might be able to sustain high ammonia levels, but non-vascular plants, fungi and lichens could be put under high risk.

Damaging impacts on ground flora, non-vascular plants and fungi have been well-documented in the proximity of livestock housing NH_3 sources. In forests and woodlands near livestock farms in Scotland, for example, Pitcairn et al. (1998) observed dramatic decline in percentage cover of ground flora species, accompanying visible injury to pine and spruce needles, an abundance of 'weed' species and high foliar N and N content of mosses, ferns and herbs (at NH_3 concentrations of 1.6–59 μg m^{-3}). Sutton (2007) and Sutton et al. (2011) observed apparent signs of injury to moss and lichen species, loss of *Sphagnum* mosses and *Cladonia* lichens and overabundance of nitrophilic ground flora species in an ecologically sensitive woodland and bog near a poultry farm in Northern Ireland. More recently, Manninen et al. (2023) have reported a decline in oligotrophic acidophyte lichen abundance in Finnish roadside woodlands at modest NH_3 and NO_2 concentrations (0–3.3 and 4–33 μg m^{-3}, respectively).

As a key mode of nitrogen (N) pollution, the dry deposition of NH_3 on soil and vegetation surfaces is difficult to measure directly and is often inferred with models using the electrical resistance analogy. Dry deposition resistance modelling has evolved over time as models have transitioned from simplistic 'big-leaf' models to more descriptive multi-layer models. Big-leaf models such as those described by Baldocchi et al. (1987) and Hicks et al. (1987) consider the entire canopy as a single leaf and provide a holistic overview of dry deposition rates over a large spatial scale. However, they provide limited insights on deposition processes occurring within the canopy layers and soil surface. In forests, the application of big-leaf models is further restricted because forest canopy layers are more complex than grasslands or croplands. Multi-layer models incorporate a greater number of processes and provide a more detailed understanding of dry deposition mechanisms over different surfaces across canopy layers (Fournier et al., 2002; Meyers et al., 1998; Nemitz et al., 2000b, 2001). Multi-layer models, however, remain poorly constrained by existing measurements and their application requires a greater number of input parameters, the measurement of which requires elaborate instrumentation and measurement of micrometeorological conditions.

Resistance models have also gradually evolved to represent the dry deposition process from unidirectional deposition to bi-directional exchange after realisation of the NH_3 re-emission potential off leaves and soil. Under certain conditions, leaves (Farquhar et al., 1980; Parton et al., 1988) and soils (Dawson, 1977; Langford et al., 1992) can re-emit the absorbed NH_3 back into the atmosphere, a phenomenon that is described using a stomatal compensation point and soil emission potential, which are incorporated into resistance models. Canopy compensation point models simplify resistance modelling and increase their accuracy by taking into account stomatal compensation points, soil emission potential and multiple resistances in a comprehensive manner. The resultant canopy compensation point (average NH_3 concentration within a canopy at zero flux) is then used to calculate dry deposition

rates (Sutton et al., 1993a, 1993b, 1995b, 1998a; Nemitz et al., 2000b, 2001; Ramsay et al., 2021; Walker et al., 2008).

Most field experiments aimed at understanding the effects of elevated N deposition involve addition of known quantities of wet solutions or fertilizer at regular intervals. For example, in several studies conducted at an experimental forest in Sweden, such as Gundale et al. (2011) and Forsmark et al. (2021), fixed quantities of ammonium nitrate are added to the study plots in the same month every year. Although this simulates N enrichment in the system, it does not capture the continuous effects of meteorology, stomatal uptake, seasonality, the interaction of the pollutant with canopy surfaces, etc. Dry deposition is a strongly climate and wind-controlled process and most field experiments fail to replicate real-world deposition conditions. Theobald et al. (2001) developed an NH_3 enhancement system which was a gas release manifold to represent NH_3 emission from a small side-ventilated poultry unit (standardised at a density of 24,000 chickens). It was placed just outside a woodland that represented a shelterbelt in order to assess NH_3 recapture by farm woodlands. Leith et al. (2004) modified this system for application in understanding NH_3 dry deposition impacts on moorland vegetation. In the present study, we describe the establishment and testing of an automated NH_3 enhancement system at two woodland locations, with appropriate meteorological and NH_3 measurements to apply a multi-layer bi-direction inferential model and quantify net ammonia deposition to different parts of the forest canopy.

The system we describe is activated under specified wind conditions to enhance ambient NH_3 concentrations at two contrasting sites, one in southern Scotland (UK) and one in central Sri Lanka (South Asia). The facilities create downwind ammonia gradients *in situ* as a basis to assess impacts of concentration and dose on species and ecosystem functions, including ground flora, non-vascular plants and fungi, impacts on soil, and chemical cycling. This paper first describes the detailed experimental design testing and optimization, including the NH_3 monitoring setup aimed at understanding lateral and vertical NH_3 movement, deposition pathways and local deposition inputs. For this purpose, the UK site acted as a test location for system calibration, optimization and to understand N impacts to sensitive UK species. The Sri Lankan site is a typical tropical forest remnant in a disturbed south Asian landscape, approximately 0.4 km from tea plantations where chemical fertilizers are applied. The understanding of NH_3 deposition pathways and planned N impacts assessments on Sri Lankan species make the findings potentially applicable to a large geographical region.

Detailed attention is given here to describing a modified version of the canopy compensation point model to estimate NH_3 dry deposition across multiple layers within the forest canopies. The modification accounts for dry deposition from a source located within the canopy, as opposed to above-canopy atmospheric deposition, which has been the focus of most previous studies.

2. Methods

2.1. Study areas

The field sites in the UK and Sri Lanka have contrasting climatic, topographical and ecological conditions that enable the testing of the ammonia enhancement system under a range of conditions.

The UK site (55°51′13″ N, 3°12′56″ W; 186 m asl) is located at Glencorse, in southeast Scotland (Fig. 1a) (hereafter referred to as Glencorse). The area was converted to a planted deciduous forest from a pasture in 1984 covering an area of 12 ha. The study plot is situated in a plantation of Silver Birch (*Betula pendula*) and Downy Birch (*Betula pubescens*), with other planted tree species including Red Alder (*Alnus rubra*), Lodgepole Pine (*Pinus contorta*), Goat Willow (*Salix caprea*) and Sitka Spruce (*Picea sitchensis*) in the vicinity of the plot. The most common moss species on the trees are *Hypnum cupressiforme* and *Eurynchium praelongum*, while the ground flora consists mostly of grasses. The soil type is mineral gley with parent material derived from carboniferous sandstones, shales and limestones (National Soil Map of Scotland, The James Hutton Institute). A leaf area density (LAD) profile of the tree canopy measured at this site using airborne Lidar is shown in Fig. 2c.

The Sri Lankan site (6°58′9″ N, 80°35′28″ E; 1645 m asl) is located in the Queensberry Tea Estate, in tropical sub-montane forests of the Rilagala Forest Reserve, Kandy district (Fig. 1b) (hereafter referred to as Queensberry). The contiguous forested area in which the study plot is located covers an area of 570 ha. The study plot is located on a hill, with two taller hills adjacent to the east and west and with downward slopes to the north and south. The evergreen vegetation has mixed characteristics of lowland rainforest and montane forest. Tree species diversity is high with at least 40 species identified. *Syzygium aqueum*, *Litsea gardneri, Cinnamomum ovalifolium* and *Symplocos cordifolia* are the most abundant tree species with 25%, 9.5%, 9% and 8% estimated abundance, respectively (B. Weerakoon et al., unpublished data). Vascular plants

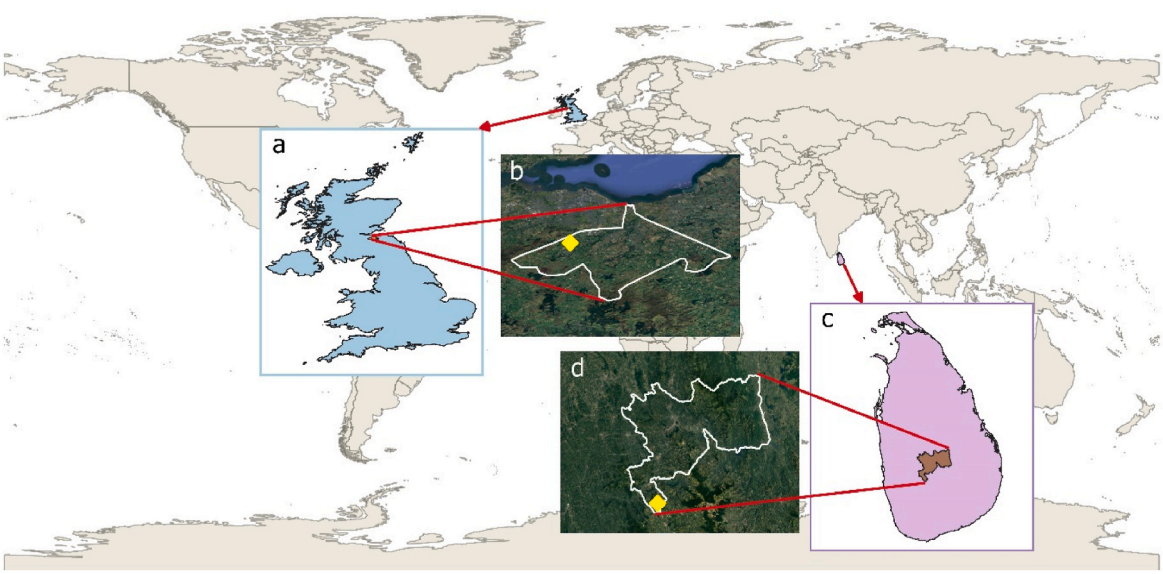

Fig. 1. (a) Glencorse is located in south-eastern Scotland in (b) Midlothian County near Edinburgh, UK. (c) Queensberry is located in (d) Kandy District of Central Province, Sri Lanka.

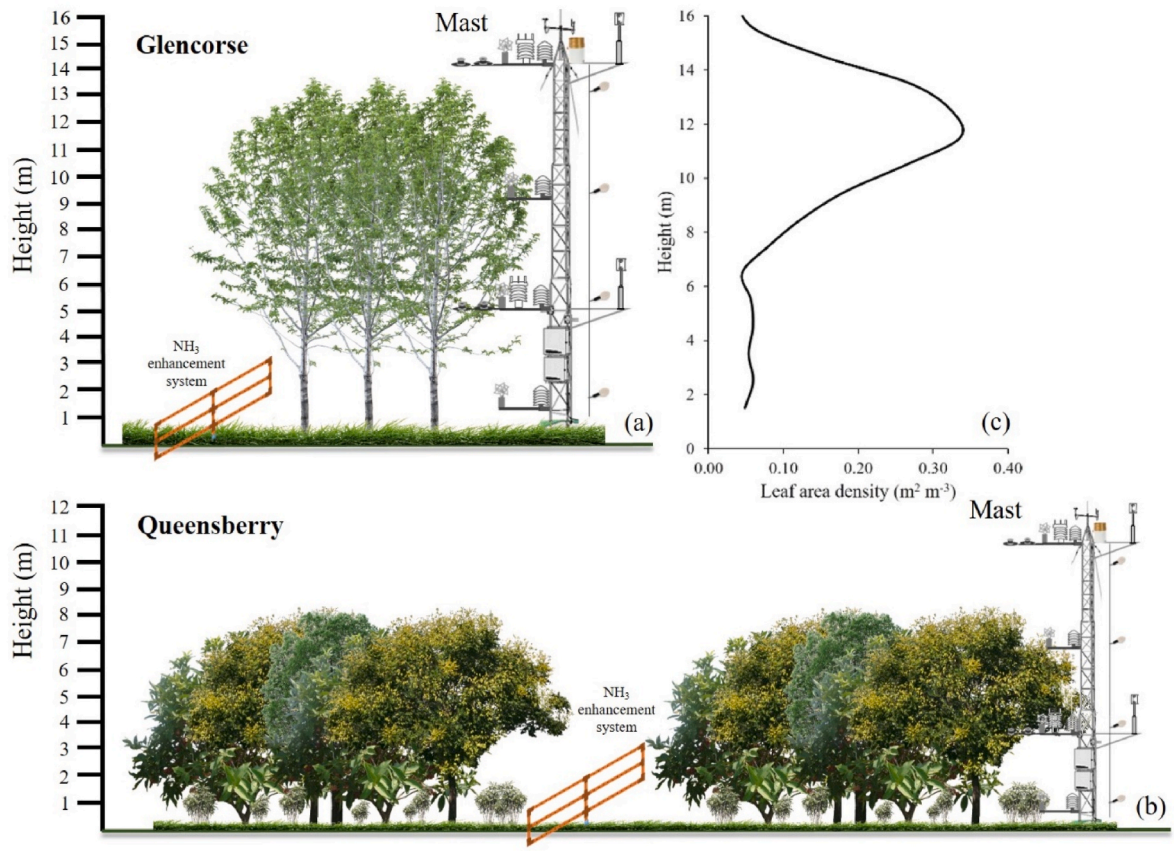

Fig. 2. The relative difference in the canopy structure at the two sites along with the height and experimental design of NH_3 enhancement with meteorological monitoring (a and b). Leaf area density of the tree canopy at Glencorse site is shown in the inset (c). LAD profile was not determined in Queensberry because of unavailability of appropriate sensors.

dominate the ground flora and large species diversity of bryophytes and lichens has been observed. At least 38 lichen species have been recorded in the study plot (B. Weerakoon et al., unpublished data), including some newly discovered and endemic lichen species (Weerakoon and Aptroot, 2014). The forest is adjacent to tea plantations of the Queensberry Tea Estate, with the study plot located 0.4 km from the forest edge. Soils are classified as red-yellow Podzolic soils within steeply dissected, hilly and rolling terrain (Subhasinghe, 1988). Overall canopy height is variable because of the undulating terrain and the variable tree species composition. Fig. 2 shows a schematic of the differences in canopy structures at the two sites and their relative heights.

2.2. Modelling NH_3 concentrations over Sri Lanka

The European Monitoring and Evaluation Programme (EMEP) model was used to estimate NH_3 concentrations over Sri Lanka. The EMEP-WRF model used here is a regional Atmospheric Chemistry Transport Model (ACTM) based on version rv4.45 (www.emep.int) of the EMEP MSC-W model which is described in Simpson et al. (2012). A detailed description of the EMEP-WRF model is given in Vieno et al. (2016) and its global application in Ge et al. (2021). The meteorological driver in the EMEP-WRF model is the Weather Research and Forecast (WRF) model version 4.2.2 (www.wrf-model.org). The horizontal resolution of the EMEP-WRF model is $1^o \times 1^o$ for the global domain and $0.11^o \times 0.11^o$ for the South Asian domain. The emissions used here are calculated for the South Asian Nitrogen Hub (SANH) project for 2015 (see Table 1).

2.3. Meteorological measurements

At both experimental sites, a suit of meteorological instruments were installed on a mast. Reflecting canopy height, the Glencorse mast is 16 m tall, while the Queensberry mast is 12 m, thereby extending 2 m and 5 m above the canopy, respectively (Fig. 2). Identical instruments with same configurations are used at both sites to minimise instrument-related uncertainties. Multi-height measurements of air temperature, relative humidity, precipitation (bulk and throughfall), leaf wetness, wind components, global solar radiation, photosynthetically active radiation (PAR), atmospheric pressure, soil volumetric water content (VWC), temperature and electrical conductivity are recorded using a CR3000 Micrologger (Campbell Scientific Ltd., Loughborough, UK) at 0.05 Hz. Wind components from the 3D sonic anemometer are recorded at 10 Hz. To minimise the uncertainty in throughfall measurements, a multi-funnel system is attached to tipping bucket rain gauges (see Table 2 for models), wherein rainwater is fed into the rain gauge through four funnels of the same diameter as the rain gauge. Throughfall data in the output is divided by four to correct for the larger surface area sampled.

Table 1
Site characteristics of the study locations.

	Glencorse, UK	Queensberry, Sri Lanka
Elevation	186 m	1645 m
Mean annual temperature	9 °C	25 °C
Mean annual rainfall	920 mm	2220 mm
Dimensions of study plot	60 m × 84 m	40 m × 120 m
Leaf area index:		
Understorey	2.3 (spring), 1.1 (summer)	5.9
Tree canopy	2.4 (spring), 1.8 (summer)	4.0
Mean canopy heights:		
Understorey	0.7 m	1.2 m
Tree canopy	14 m	8 m

Table 2
Meteorological and physical parameters measured at both the sites and instrument heights.

Instrument	Manufacturer	Measurement	Height/Depth (m)	
			Glencorse	Queensberry
A100/A100R cup anemometer	Vector Instruments	Wind speed (m s^{-1})	0.5, 2.2, 7.2, 12.3	0.1, 2.2, 5.7, 11.2
HMP60 temperature and humidity probe	Vaisala	Air temperature (°C), relative humidity (%)	0.5, 2.0, 7.1, 12.4	0.2, 2.6, 5.5, 11.3
LWS leaf wetness sensor	METER Environment	Leaf wetness (mV)	0.5, 2.0, 7.1, 11.6	0.3, 2.0, 3.6, 5.6
WXT536 weather transmitter	Vaisala	Air temperature (°C), relative humidity (%), atm. pressure (mbar), wind speed (m s^{-1}), wind direction (°), rainfall (mm)	2.3, 15.6	2.5, 11.4
SP1110 Pyranometer	Skye Instruments	Global solar radiation (W m^{-2}, kJ m^{-2})	2.0, 15.1	2.7, 11.0
SKP215 Quantum sensor	Skye Instruments	PAR (μmol m^{-2})	2.0, 15.1	2.7, 11.0
Windmaster Pro 3D sonic anemometer	Gill Instruments	UVW wind vectors	2.7, 16.2	3.0, 12.4
TB4MM tipping bucket rain gage	HS Hyquest Solutions	Rainfall (mm)	–	12.0
ARG314 tipping bucket rain gauge	Environmental Measurements Limited	Rainfall (mm)	12.0	0.46
ARG100 tipping bucket rain gauge	Environmental Measurements Limited	Rainfall (mm)	0.34	–
CS655 water content reflectometer	Campbell Scientific	Soil VWC (m^3 m^{-3}), temperature (°C) and electrical conductivity (dS m^{-1})	−0.05, −0.10, −0.15	−0.05, −0.10, −0.15

3D sonic anemometer data is stored at 10 Hz, while all other meteorological data is averaged to 15-min. A detailed listing of the collected measurements is given in Table 2.

To characterize the vertical wind profile within the canopy and to parameterize conditions such as speed and friction velocity (u^*) with respect to above-canopy conditions, two campaigns were conducted at Glencorse (during growing season and post-senescence) and one in Queensberry, wherein a 3D sonic anemometer was sequentially installed at 4 heights between ground-level and top of the canopy and allowed to run for 48 hours at each height. The measurements were then referenced to measurements from the second sonic anemometer installed above the canopy.

2.4. Ammonia enhancement system

The ammonia enhancement system is made up of a fan, a controlled ammonia source and a manifold to release the gas. The manifold is constructed from three 20 m long 110 mm diameter (OD) PVC tubes placed horizontally parallel to each other at 0.5, 1.35 and 2.2 m above the ground (Fig. 3). Along the length of each tube at 20 cm intervals, six 4 mm diameter holes were drilled around the entire circumference of the tube. The three height increments allow the gas to propagate uniformly along the soil surface, understorey, trunk space and the lower tree canopy. An ACM200 fan (Vent-Axia, Manor Royal, UK) was installed at the centre of the manifold which generates a positive pressure airflow into the manifold tubes achieving an effective flow rate of 8 l min^{-1} from the holes along the tubes' length. A 6.35 mm diameter stainless steel pipe conducts pure anhydrous ammonia from a cylinder placed on one end of the manifold via a G-series mass flow controller (MFC; calibrated for 0–10 l min^{-1} NH_3) (MKS Instruments, Andover, MA, USA) and a Type 6027 solenoid valve (Bürkert Fluid Control Systems, Cirencester, UK) and injects the gas into the fan airflow which dilutes the ammonia and releases it through the tubes. A 170 PC pressure sensor (Honeywell Safety and Productivity Solutions, Morris Plains, NJ, USA) constantly measures the difference in air pressure generated by the airflow in the release manifold and the outside air pressure. In case of a fan failure or physical damage to the tubes, the fall in pressure difference is detected by the sensor, which closes the solenoid valve. Additionally, to prevent accidental release of pure ammonia, the solenoid valve shuts down in the event of a power failure. This entire setup is connected to the CR3000 Micrologger at the meteorological mast. NH_3 flow and MFC status data is averaged to 1-min in the output.

The enhancement system at Glencorse is controlled to have a unidirectional NH_3 release (wind direction being from the predominant SW

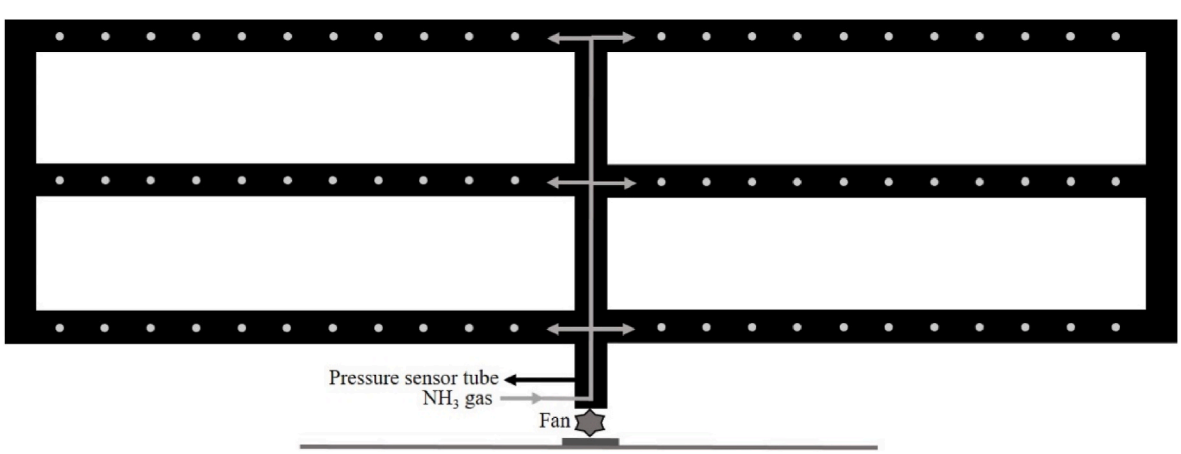

Fig. 3. Structure of the NH_3 enhancement system release manifold with PVC tubes with holes (6 around the pipe circumference). Direction of NH_3 flow is shown by the grey arrow.

wind sector, 275–345°) because of constrained plot boundaries, while it is released bi-directionally in Queensberry (wind direction from alternate sectors 5-75° (southwestern transect) and 185–255° (northeastern transect)) (Fig. 4). At Queensberry, the aim of this design was to increase the probability of NH_3 release within the plot, given the occurrence of SW and NE prevailing winds in different seasons. Consideration of prior meteorological data suggested that wind directions are more variable seasonally due to changeable monsoon winds. Moreover, the site is located on a hill resulting in higher turbulence and variable wind directions. The bi-directional NH_3 release therefore helps to align NH_3 enhancement with these variations. The Glencorse system became operational in September 2021, while the Queensberry experiment started in March 2022.

At both sites, to maintain uniform NH_3 release and resultant deposition at different wind speeds, release occurs at three levels controlled by the MFC. To counteract the dilution effect, NH_3 release gradually increases with wind speed at predetermined rates at Glencorse (0.3–0.8 m s^{-1}: 0.2 l min^{-1}, 0.8–1.2 m s^{-1}: 0.3 l min^{-1} and 1.2–10 m s^{-1}: 0.5 l min^{-1}) and Queensberry (0.3–0.8 m s^{-1}: 0.3 l min^{-1}, 0.8–1.2 m s^{-1}: 0.5 l min^{-1} and 1.2–10 m s^{-1}: 0.9 l min^{-1}). If wind direction is within the set sectors, and if these wind speed conditions are met for a 1-min period by the below-canopy WXT 536 weather transmitter, then the micrologger opens the solenoid valve and NH_3 is released at the specified rate. Irrespective of appropriate wind directions, NH_3 is not released at wind speeds <0.3 m s^{-1} to prevent the gas from building up under the canopy, nor at wind speeds >10 m s^{-1} to prevent wasting NH_3 during periods when the high dispersion does not allow a significant NH_3 enhancement to be generated at reasonable release rates. The volume of NH_3 released is calculated by multiplying the measured flow rate by the elapsed time during fumigation. The operational control range of the MFC is from 2% to 100% of full scale. The accuracy is ± 0.2% of full scale for flows from 2 to 20% of full scale and ± 1% of set-point for flows from 20 to 100% of full.

2.5. Ammonia concentration monitoring

Passive diffusion samplers (UKCEH Adapted Low-cost Passive High Absorption (ALPHA®) samplers) (Tang et al., 2001) were used for continuous long-term NH_3 monitoring. These passive samplers have been optimised for long-term sampling (1 month in this study) and are sensitive enough for concentrations as low as ≈0.03 μg m^{-3} and up to 100 μg m^{-3}. In an ALPHA® sampler, a filter coated with citric acid as an absorbent for NH_3 is placed inside a polyethylene sampler body. A 5 μm PTFE membrane is placed at the open face of the sampler body to standardize the path length at 6 mm enabling a turbulent-free diffusion of NH_3 through the membrane to the filter (Tang et al., 2001). Calibration of the ALPHA® samplers against active denuder sampling takes account of membrane resistance and a laminar boundary layer.

After field exposure, the ALPHA® sample acid filters are analysed using a flow injection analyser based on the salicylate method using an AA3 HR AutoAnalyzer (Seal Analytical Ltd., Wrexham, UK). Background NH_3 concentrations were measured at Glencorse from January–August 2021 using triplicate ALPHA® samplers 1.5 m above the ground. After installation of the enhancement system in September 2021, the background concentration continued to be measured in the upwind direction of the release (Fig. 4a). In Queensberry, background concentrations were measured in March 2020 and then starting April 2022 using ALPHA® samplers in opposite direction from the NH_3 release sectors and placed along the plot boundary after installation of the enhancement system (Fig. 4b).

NH_3 concentrations in the direction of the release were measured along a 44 m transect at Glencorse (Fig. 4a) and two transects in Queensberry of 24 m and 32 m lengths (Fig. 4b). Sampling points were selected along the transect based on previous studies (Leith et al., 2004; Sheppard et al., 2011; Theobald et al., 2001). ALPHA® samplers were fixed to 1.5 m tall posts at distances of 2, 4, 6, 8, 16, 24, 32 and 44 m from the release system.

At Glencorse, in addition to the transect, 39 ALPHA® samplers were deployed at 13 heights (0.05, 0.25, 0.5, 0.75, 1, 1.25, 1.5, 1.75, 2, 2.25, 2.5, 3 and 3.5 m above ground) on 3.5 m tall poles at three distances along the downwind transect (4, 10 and 16 m) to measure the vertical NH_3 concentration profile following release from the manifold. The vertical array of ALPHA® samplers was deployed over a one-year period. Ambient NH_3 concentration above 3.5 m was assumed to be equal to the concentration measured at 3.5 m while modelling NH_3 dry deposition.

A G2123 NH_3/H_2O Analyser (Picarro, Santa Clara, CA, USA) (Martin et al., 2016) was deployed at both sites in two separate campaigns to report real-time NH_3 concentrations. The Glencorse campaign was conducted from 9th to 19th November 2021, while the Queensberry campaign lasted from 24th March to 3rd April 2022. This allowed optimization of NH_3 release rates from the fumigation systems in order to achieve the target enhancement concentrations. At Queensberry, this also allowed characterization of vertical NH_3 concentration profiling in absence of vertical ALPHA® sampler arrays.

The Picarro analyser was placed 10 m downwind from the release manifold along the transect, housed in a custom-built air-conditioned enclosure. Air was sampled at four heights (0.5, 1, 1.5 and 2.5 m) from the ground using a custom-designed sampling system. Sampling was carried out for 2 min at each height via a valve manifold, controlled automatically through a LabVIEW computer program (National Instruments Corp., Austin, TX, USA). All four sampling inlets were 5.5 m long, made using PTFE tubing (1/4 inch external diameter, 1/8 inch internal diameter). The sampling system temperature was maintained at ~40 °C (± 3 °C) using self-regulating heating tape and insulation. Sample lines were continuously purged at a flow rate of 7 standard l min^{-1} between sampling for 1 min and 12 standard l min^{-1} during sampling. The inlet temperature, airflow and PTFE tubing are set up to minimise delays while the analyser adjusts to the concentration of a new switching height due to NH_3 adsorption/desorption on inlet surfaces. However, it is expected that some lag effect would still be introduced in the common lines of the switching system, especially when switching between high and low NH_3 concentrations. Whilst the heating may cause some volatilisation of volatile ammonium nitrate (NH_4NO_3) aerosol, the

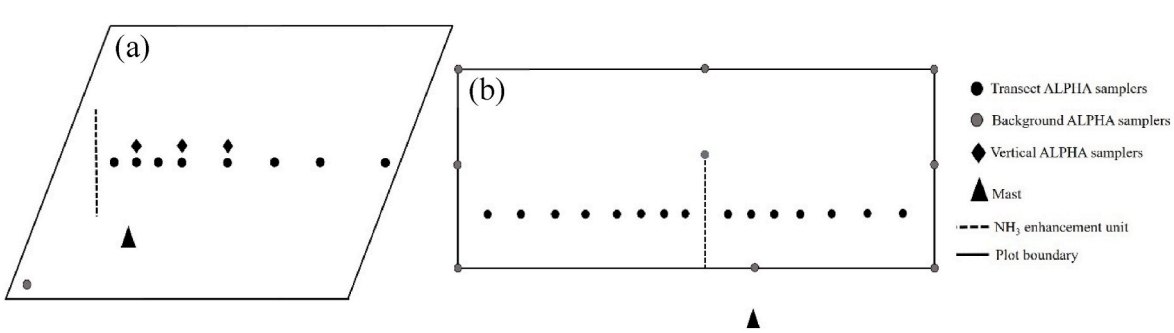

Fig. 4. Distribution of ALPHA® samplers and the experiment setup at (a) Glencorse and (b) Queensberry as seen from above.

NH_4NO_3 field would be expected to be smooth and the volatilisation would be expected to generate a relatively constant background.

2.6. Calculation of dry deposition

A common approach to estimating the dry deposition process of a pollutant such as NH_3 is by analogy to Ohm's Law that relates the electric flux to the driving potential (here the concentration difference) and a resistance. Its simplified form can be represented as Eq. (1) (Fowler, 1978; Wesely and Hicks, 1977):

$$F_\chi(z) = \frac{\chi_a}{R_t}, \quad (1)$$

where F_χ = deposition flux at height z, χ_a = ambient NH_3 concentration at height z, and R_t = total resistance to NH_3 dry deposition (i.e. inverse of deposition velocity ($V_d = 1/R_t$)). The total resistance for dry deposition is caused by air turbulence, boundary layers, surface conditions and stomatal activity, and can be estimated based on measurement of micrometeorological and physiological parameters.

Dry deposition of NH_3 to surfaces is known to be a bi-directional exchange wherein leaf stomata, soil surface and the canopy as a whole can have a NH_3 re-emission potential. This exchange is represented by canopy compensation point models as the balance between ambient NH_3 concentration and the canopy compensation point, such that deposition occurs when ambient concentration exceeds the compensation point. The canopy compensation point model can be modified for specific

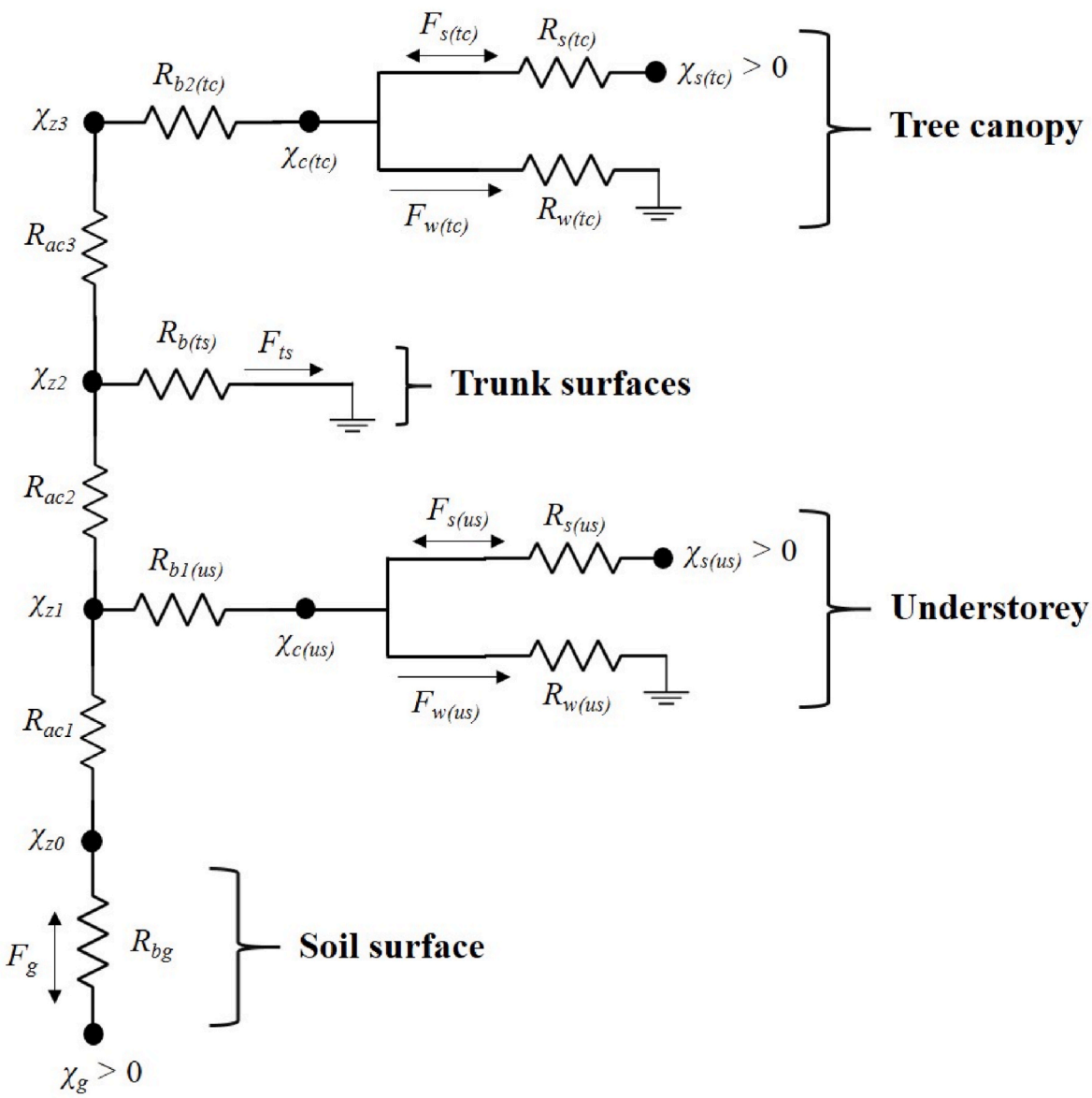

Fig. 5. Resistance diagram of the multi-layer model modified for application to a 4-layer forest canopy. R_{aci} (in-canopy aerodynamic resistances) are shown in the diagram to represent change in NH_3 concentration with height caused by in-canopy air turbulence but R_{aci} is not included in the flux calculations as it is accounted for by making direct measurements of NH_3 concentration at different heights within the canopy (χ_{zi}). $R_{b1(us)}$ and $R_{b2(tc)}$ are the boundary layer resistances around leaves in the understorey and tree canopy, respectively. $R_{b(ts)}$ is the trunk boundary layer resistance. R_{bg} is the soil boundary layer resistance. $\chi_{c(us)}$ and $\chi_{c(tc)}$ are the canopy compensation points at the understorey and tree canopy layers, respectively. $\chi_{s(us)}$ and $\chi_{s(tc)}$ are the stomatal compensation points at the understorey and tree canopy layers, respectively. χ_g is the soil compensation point. $R_{s(us)}$ and $R_{s(tc)}$ are the stomatal resistances in the understorey and tree canopy, respectively. $R_{w(us)}$ and $R_{w(tc)}$ are the cuticular resistances in the understorey and tree canopy, respectively. F_g is the deposition flux on the soil surface. $F_{s(us)}$ and $F_{s(tc)}$ are the stomatal deposition fluxes in the understorey and tree canopy, respectively. $F_{w(us)}$ and $F_{w(tc)}$ are the cuticular deposition fluxes in the understorey and tree canopy, respectively. F_{ts} is the deposition flux on trunk surfaces.

applications depending on the vegetation type, canopy structure, availability of micrometeorological measurements, etc. Normally, resistance models are used to estimate deposition on the basis of measured or modelled concentration above the canopy. Here, we drive the deposition with concentrations generated and measured within the canopy and the model is adapted accordingly.

We applied the model to multiple layers of the forest canopy and estimated NH_3 deposition fluxes to each layer individually by calculating appropriate resistances and compensation points (Fig. 5). The forest canopy was divided into four layers: soil surface, understorey (including forest floor) (us), trunk surfaces (ts) and tree canopy (tc). Height ranges (z_i) for each layer are given in Table 3. For understorey and tree canopy, canopy resistance is made up of the quasi-laminar boundary layer resistance (R_b), stomatal resistance (R_s) and cuticular resistance (R_w), while the soil surface boundary layer resistance (R_{bg}) and trunk boundary layer resistance (R_{bts}) are considered for the soil surface and trunk surfaces, respectively. While compensation points are considered for leaf stomata and soil surface due to their NH_3 re-emission potential, plant cuticles and tree trunks are considered here to be chemically inert. Because we start with the NH_3 concentrations (χ_{zi}) within each canopy layer we do not need to account for vertical turbulent transport (typically parametrised through the atmospheric aerodynamic resistance, R_a, above the canopy, and the in-canopy turbulent transport, R_{ac}, within) and resistance due to turbulent transport to the leaf itself becomes insignificant compared with the R_b terms.

2.6.1. Resistance calculations

2.6.1.1. Quasi-laminar boundary layer resistances (R_b and $R_{b(ts)}$). A generalised form of resistance for diffusion of a gas through the quasi-laminar boundary layer around surfaces is given by Owen and Thomson (1963):

$$R_b \text{and } R_{b(ts)} = (Bu_*)^{-1}, \tag{2}$$

where R_b is the boundary layer resistance around leaves, $R_{b(ts)}$ is the boundary layer resistance around trunk surfaces, u^* is the friction velocity, and the sub-layer Stanton number (B) is a function of the Schmidt (Sc) number for NH_3 (≈ 0.57), which is linked to the molecular diffusivity of the gas, and the Reynolds number (Re^*) which can be determined from the kinematic viscosity of air (ν_a), the roughness length of the canopy (z_0) and u^*:

$$Re_* = z_0 u_* / \nu_a \tag{3}$$

The boundary layer resistance around leaves (R_b) was calculated using a commonly used parameterisation for B given by Chamberlain (1966) as:

$$B^{-1} = 1.45 Re_*^{0.24} Sc^{0.8} \text{ (for leaves)} \tag{4}$$

The trunk boundary layer resistance ($R_{b(ts)}$) was also calculated using Eq. (2) but with a different parameterisation for B. Parameterisations for estimating dry deposition flux of pollutants on tree trunks, stems and branches are rare. The boundary layer or surface resistance to dry deposition on woody surfaces are usually included in the total canopy-level formulation of the resistance and not determined separately. Some studies such as Murphy and Sigmon (1990) have suggested that due to the chemical inertness of wood, its surface resistance could be roughly four times than that of leaves. However, evidence of the accuracy of this generalization based on bark roughness, u^*, gas properties, trunk size, etc. is lacking. provided a parameterisation (Eq. (5)) for determining the Stanton number for bluff bodies like cylinders and half cylinders. Their parameterisation was tested in wind tunnel experiments and found to be consistent in studies such as Chamberlain (1968) and Chamberlain et al. (1984). We applied this relation for calculating $R_{b(ts)}$:

$$B^{-1} = 2.4 Re_*^{0.45} Sc^{0.8} \text{ (for trunk)} \tag{5}$$

2.6.1.2. Soil surface boundary layer resistance. The quasi-laminar boundary layer resistance of the soil surface (R_{bg}) was calculated using the relation formulated by Schuepp (1977):

$$R_{bg}^{-1} = \frac{k u_{*g}}{S_c - \ln(\delta_0 / z_1)}, \tag{6}$$

where k is the Karman constant ($\approx$0.41), u_{*g} is the friction velocity at the ground level (m s^{-1}), $\delta_0 = D_\chi/(k\, u_{*g})$ is the distance above ground where molecular diffusivity of NH_3 (D_χ) equals the eddy diffusivity, with $D_\chi = \nu_a/Sc$ and z_1 is the upper height of the logarithmic wind profile that forms above the ground of which u_{*g}/k is the slope (here assumed to be 0.1 m consistent with Schuepp (1977) and Nemitz et al. (2001).

The value of the friction velocity at the ground surface u_{*g} was estimated using a relationship between u^* measured just above the soil surface with above-canopy u^* during the vertical wind profiling campaigns. It was found that u_{*g} could be approximated by above-canopy $u^*/3.4$ at Queensberry and above-canopy $u^*/6.2$ during the growing season and above-canopy $u^*/6.5$ after leaf senescence at Glencorse (Fig. 9b).

2.6.1.3. Cuticular resistance. The cuticular resistance (R_w) depends on the chemical properties of the cuticle, physiology, humidity, water saturation of the cuticle and amount of cuticular surface water. Several formulations for R_w have been derived (Flechard et al., 1999; Kruit et al., 2010; Nemitz et al., 2000b; Sutton and Fowler, 1993) and compared. However, estimates of R_w strongly vary with vegetation type, climate and background air pollution conditions and are difficult to generalise (Massad et al., 2010). Even fewer parameterisations have been applied to forest ecosystems. Therefore, we assessed three different methods to calculate R_w for a comparative analysis and one method to estimate cuticular deposition using a capacitance model.

The parameterisation derived by Sutton and Fowler (1993), is one of the most commonly used relationships for cuticular resistance. It is an exponential curved function of relative humidity (RH) but independent of ambient NH_3 concentration:

$$R_w = R_{w(\min)} \times \exp(a(100 - RH)) \tag{7}$$

RH controls the thickness of water films that form on cuticles and other non-stomatal surfaces, which are strong NH_3 sinks (Flechard et al., 1999; Sutton et al., 1995a). However, R_w has also been found to be dependent on temperature (Flechard et al., 2010) and leaf area index (LAI) (Zhang et al., 2003), which is taken into account by Massad et al. (2010) by providing an expanded, more generalised, equation for R_w:

$$R_w = \frac{R_{w(min)} \times \exp(a(100 - RH)) \times \exp(0.15T)}{(LAI)^{0.5}} \tag{8}$$

where, $R_{w(min)}$ is the minimum R_w constrained by the parameterisation (2 s m^{-1}), a is a scaling factor set at 0.031 (mean value from forest studies (Massad et al., 2010)), T is the air temperature (^{o}C) and LAI is the one-sided leaf area index (m^2 m^{-2}). We use eq. (8) as our **first** parameterisation.

The **second** parameterisation, by Jones et al. (2007a) for semi-natural moorland vegetation, distinguishes between day-time (solar radiation >5 W m^{-2}) (Eq. (9a)) and night-time (solar radiation

Table 3
Height zones of each of the four layers for both the sites.

Layer	Dominant surface	Height range (m)	
		Glencorse	Queensberry
Soil surface	Soil	0	0
Understory	Grasses	0–1.3	0–1.3
Trunk space	Wood	0.4–2.9	0.3–3.1
Tree canopy	Leaves	2.9–14.0	3.1–8.0

<5 W m^{-2}) (Eq. (9b)) to account for diurnal micrometeorological differences and also NH_3 saturation of cuticles caused by high ambient concentrations. The LAI-dependency, as accounted for by Zhang et al. (2003) and Massad et al. (2010), was added to this parameterisation to account for leaf phenology, varying canopy architecture and differences in leaf surface area between understorey vegetation and the tree canopy.

$$R_w(day) = \frac{(a \times Ambient\ NH_3\ concentration) + b}{(LAI)^{0.5}} \tag{9a}$$

$$R_w(night) = \frac{(c \times Ambient\ NH_3\ concentration) + d}{(LAI)^{0.5}}, \tag{9b}$$

where the values of constants are $a = 1.05$, $b = 3.6$, $c = 1.13$ and $d = 4.6$.

The **third** parameterisation is the one employed in the DEPAC (DEPosition of Acidifying Compounds) module (van Zanten et al., 2010) (Eq. (11)) in the Netherlands. In this parameterisation, similar to the stomatal compensation point, the cuticular flux is derived from the difference between gaseous NH_3 concentration at the external leaf surface water interface (χ_w) and the canopy compensation point (χ_c), where the values of R_w and χ_w are estimated as follows:

$$F_w = \frac{\chi_c - \chi_w}{R_w} \tag{10}$$

$$R_w = \frac{LAI_{Haarweg}}{LAI} \times \alpha \times \exp\left(\frac{100 - RH}{\beta}\right), \tag{11}$$

where α and β are scaling coefficients ($\alpha = 2$ s m^{-1}, $\beta = 12$) and $LAI_{Haarweg}$ is the leaf area index at the Haarweg measuring site (3.5 m^2 m^{-2}). This represents an empirical fit to the Haarweg grassland study site (Kruit et al., 2010; van Zanten et al., 2010).

$$\chi_w = \left(\frac{2.75 \times 10^{15}}{T}\right)\exp\left(\frac{-1.04 \times 10^4}{T}\right)\left(1.84 \times 10^3 \times \chi_z \exp(-0.11T) - 850\right), \tag{12}$$

where T is leaf temperature (K) in DEPAC, but we use air temperature (K) and χ_z is the ambient NH_3 concentration (in μg m^{-3}) at height z.

The dynamic canopy compensation point-cuticular capacitance (χ_c-C_d) model derived by Sutton et al. (1998a) provides a **fourth** approach which accounts for previously deposited ammonia on the cuticle surfaces, where the wetness and acidity of the epicuticular water film determines the adsorption or desorption of the ammonia from the cuticle. The epicuticular water film acts like a capacitor with capacitance C_d:

$$C_d = \frac{Q_d}{\chi_d}, \tag{13}$$

where Q_d is the adsorption charge (μg m^{-2}) and χ_d is the concentration associated with the capacitor (μg m^{-3}).

C_d can be estimated using a solubility equilibria derived from the Henry equilibrium constant and an equivalent canopy area water-film thickness ($M^c_{H_2O}$) (Sutton et al., 1995a, 1998a):

$$C_d = M^C_{H_2O}\frac{[NH_4^+] + [NH_3.H_2O]}{[NH_3]_{(g)}} \tag{14}$$

$$C_d = M^C_{H_2O}\left[\frac{[H^+]}{10^{\left(1.6035 - \left(\frac{4207.6}{T}\right)\right)}} + 10^{\left(\left(\frac{1477.7}{T}\right) - 1.6937\right)}\right], \tag{15}$$

where C_d and $M^c_{H_2O}$ are in metres and T is air temperature in Kelvin. H^+ is calculated from leaf pH (assumed value of 4.5).

$$M^c_{H_2O} = LAI \times 20 \times \exp\left(\frac{[H - 60]}{10}\right), \tag{16}$$

where $M^c_{H_2O}$ is in nm and H is relative humidity (%).

The model requires an initial value of either Q_d ($Q_{d\{i\}}$). The new capacitance charge after t seconds is then:

$$Q_{d\{i+t\}} = Q_d - (F_d.t) + Q_{d\{i\}}K_r \tag{17}$$

$$F_d = \frac{(\chi_C - \chi_d)}{R_d}, \tag{18}$$

where F_d is the flux entering or leaving the capacitor, K_r is a rate reaction constant that accounts for net removal of NH_3 by leaf surfaces (−0.01 s^{-1}), χ_c is the canopy compensation point and R_d is the charging resistance of the capacitor which is derived as $R_d = 5000/C_d$ and scaled for LAI as:

$$R_d = \left(\frac{5000}{C_d}\right) \Big/ (LAI)^{0.5} \tag{19}$$

Using the new value of Q_d obtained from eq. (17), χ_d is calculated using eq. (13) and the process is repeated for subsequent time steps.

2.6.1.4. Stomatal resistance. The stomatal resistance (R_s) is a result of resistance to NH_3 deposition on leaves caused by stomatal closure, which is dependent on temperature, humidity, vapour pressure deficit, radiation, plant physiology and soil water conditions. Therefore, R_s is treated similarly to CO_2 and H_2O transfer, which makes it easier to estimate than R_w. We use the parameterisation given by Nemitz et al. (2001) that accounts for water vapour transfer during daytime, secondary effects of water stress and relative humidity (Jarvis, 1976) and the uncertainty at dawn and dusk due to low and variable light levels. The parameterisation is eventually scaled and reduced to:

$$R_s = \min\left[R_{sMax}, R_{sMin}\left(1 + \frac{\alpha_1}{Rad}\right)\right], \tag{20}$$

where $R_{sMax} = 5000$ s m^{-1}, $R_{sMin} = 35$ s m^{-1}, α = 180 W m^{-2} and Rad = solar radiation (W m^{-2}).

Similar to cuticular resistance parameterisations, an LAI dependency was added to the R_s parameterisation to account for seasonal variations and differences in canopy architecture with separate LAI values used for the understory and tree canopy:

$$R_s = \min\left[R_{sMax}, R_{sMin}\left(1 + \frac{\alpha_1}{Rad}\right)\right] \Big/ (LAI)^{0.5} \tag{21}$$

2.6.2. Stomatal (χ_s) and soil (χ_g) compensation points

Leaves can emit NH_3 and act as a source depending on the ratio of ambient NH_3 concentration to stomatal NH_3 concentration (Farquhar et al., 1980; Husted and Schjoerring, 1995). This is dependent on canopy temperature and the ratio of ammonium and hydrogen ion concentration in the leaf apoplast or stomatal emission potential ($\Gamma_s = [NH_4^+]/[H^+]$) (Nemitz et al., 2000a). Similarly, soil temperature and the equilibrium between NH_3 and NH_4^+ in the soil pore space determines the switching of soil from NH_3 sink to source. The soil emission potential is calculated as the ratio of soil NH_4^+ concentration (top 5 cm) to H^+ concentration (calculated from soil pH) ($\Gamma_g = [NH_4^+]/[H^+]$). After determining Γ_s and Γ_g values, χ_s and χ_g are estimated using parameterisation derived by Sutton et al. (1994) and reformulated by Nemitz et al. (2001):

$$\chi_s\ and\ \chi_g = \frac{161500}{T}\exp\left(-\frac{10380}{T}\right)\frac{[NH_4^+]}{[H^+]}, \tag{22}$$

where T is the canopy or soil temperature (°C). $[NH_4^+]$ = concentration of NH_4^+ ions (μmol l^{-1}) and $[H^+]$ = concentration of H^+ ions (μmol l^{-1}).

In this study, to estimate Γ_g, we sampled 10 cm topsoil from 36 points in April 2022. 15 g subsamples were extracted in 50 ml of 1M KCl solution. NH_4^+ concentration was measured using colorimetry (AQ2 discrete analyser, Seal Analytical). KCl extractable NH_4^+ is probably

larger than the NH_4^+ that governs Γ_g, however, we were constrained by the resources available. 10 g subsamples dissolved in 20 ml of deionised water were used to measure pH using an MP 220 pH meter (Mettler Toledo, Columbus, OH, USA) for estimating H^+ concentration (G. Toteva et al., unpublished data).

Stomatal emission potential (Γ_s) was estimated using the Aerodynamic Gradient Method (AGM) by measuring vertical concentration gradients of ammonia above the forest floor. This method estimates fluxes based on Fick's law and the Monin–Obukhov similarity theory assuming a constant flux layer. The flux F_χ can be calculated from the logarithmic concentration profile as (Garland, 1977; Sutton et al., 1992):

$$F_\chi = -\frac{u_* k(c_2 - c_1)}{\ln\left(\frac{z_2-d}{z_1-d}\right) - \psi_H\left(\frac{z_2-d}{L}\right) + \psi_H\left(\frac{z_1-d}{L}\right)}, \tag{23}$$

where c_2 and c_1 are the NH_3 concentration measurement heights at z_2 and z_1, respectively, d is the displacement height, L is the Monin-Obukhov length and ψ_H is the integrated stability correction function for heat and inert tracers which can be parameterized under the following two conditions (Thom, 1975):

For stable conditions (L > 0),

$$\psi_H = -5.2\left[\frac{z-d}{L}\right], \tag{24}$$

and for unstable conditions (L < 0),

$$\psi_H = 2\,ln\left(\frac{1+[1-16((z-d)/L)]^2}{2}\right) \tag{25}$$

The AGM was applied only to periods when no NH_3 had been released from the manifold in the preceding 24 h to ensure that the detected vertical difference in the flux originated from and was directed to the understorey. NH_3 concentrations were recorded at two heights above ground (1.5 and 2.5 m) using a Picarro G2123 NH_3/H_2O Analyser located 10 m downwind of the source. Wind components were measured using a 3D sonic anemometer and processed at 30-min time steps using EddyPro 7 software (LI-COR Biosciences, Lincoln, NE, USA). Γ_s for the understorey (and forest floor) was estimated when the flux switched from emission to deposition under conditions when NH_3 surface exchange was expected to be driven by stomatal exchange at RH < 60% when R_w can be fairly large. Under these conditions, χ_s can be replaced with χ_a (ambient NH_3 concentration) and eq. (22) can be rearranged to estimate Γ_s (Nemitz et al., 2004; Ramsay et al., 2021). As vertical gradient measurements of NH_3 concentration above the tree canopy were not available, the values of Γ_s estimated for vegetation shorter than 1.5 m were used for all vegetation layers within the canopy.

2.6.3. Deposition fluxes

Although emissions can occur from the bidirectional model framework, with increased NH_3 concentrations downwind of the release, net deposition fluxes are expected to dominate. The component deposition fluxes of NH_3 to the different layers are calculated using the canopy compensation point model.

2.6.3.1. NH_3 exchange flux at the soil surface

$$F_g = \frac{\chi_{z0} - \chi_g}{R_{bg}}, \tag{26}$$

where F_g is the soil NH_3 exchange flux at the soil surface and χ_{z0} is ambient NH_3 concentration at the soil surface (5 cm above the ground).

2.6.3.2. Cuticular NH_3 deposition and exchange flux

$$F_{w(us)} = \frac{\chi_{c(us)}}{R_{w(us)}}, \tag{27}$$

where $F_{w(us)}$ is the cuticular deposition flux on the understorey vegetation and $\chi_{c(us)}$ is the canopy compensation point of the understorey. Cuticular deposition is estimated using eq. (27) when applying the parameterizations from Massad et al. (2010) and Jones et al. (2007a).

$$F_{w(us)} = \frac{\chi_{c(us)} - \chi_{w(us)}}{R_{w(us)}}, \tag{28}$$

where $F_{w(us)}$ = Cuticular exchange flux with the understory vegetation.

$$F_{d(us)} = \frac{\left(\chi_{c(us)} - \chi_{d(us)}\right)}{R_{d(us)}}, \tag{29}$$

where $F_{d(us)}$ = Cuticular exchange flux with the understory vegetation while the epicuticular water film acts as a capacitor.

While using the parameterizations from the DEPAC module and Sutton et al. (1998a), cuticular NH_3 exchange is estimated using eqs. (28) and (29), respectively.

Similarly, cuticular NH_3 deposition and exchange fluxes with the tree canopy are formulated as:

$$F_{w(tc)} = \frac{\chi_{c(tc)}}{R_{w(tc)}}, \tag{30}$$

where $F_{w(tc)}$ is the cuticular deposition flux on the tree canopy and $\chi_{c(tc)}$ is the canopy compensation point of the tree canopy. Cuticular deposition is estimated using eq. (30) when applying the parameterizations from Massad et al. (2010) and Jones et al. (2007a).

$$F_{w(tc)} = \frac{\chi_{c(tc)} - \chi_{w(tc)}}{R_{w(tc)}}, \tag{31}$$

where $F_{w(tc)}$ = Cuticular exchange flux with the tree canopy.

$$F_{d(tc)} = \frac{\left(\chi_{c(tc)} - \chi_{d(tc)}\right)}{R_{d(tc)}}, \tag{32}$$

where $F_{d(tc)}$ = Cuticular exchange flux with the tree canopy while the epicuticular water film acts as a capacitor.

While using the parameterizations from the DEPAC module and Sutton et al. (1998a), cuticular NH_3 exchange is estimated using eqs. (31) and (32), respectively.

2.6.3.3. Stomatal NH_3 exchange flux

$$F_{s(us)} = \frac{\chi_{c(us)} - \chi_{s(us)}}{R_{s(us)}}, \tag{33}$$

where $F_{s(us)}$ = Stomatal exchange flux with the understory vegetation.

$$F_{s(tc)} = \frac{\chi_{c(tc)} - \chi_{s(tc)}}{R_{s(tc)}}, \tag{34}$$

where $F_{s(tc)}$ = Stomatal exchange flux with the tree canopy.

2.6.3.4. NH_3 deposition flux on trunk surfaces

$$F_{ts} = \frac{\chi_{z2}}{R_{b(ts)}}, \tag{35}$$

where F_{ts} is the deposition flux to trunk surfaces and χ_{z2} is the ambient NH_3 concentration at height z_2.

2.6.3.5. Total NH_3 fluxes to the vegetation layers

$$F_{us} = F_{w(us)} + F_{s(us)} \text{ and } F_{d(us)} + F_{s(us)}, \tag{36}$$

where F_{us} = Total net deposition flux on the understorey.

$$F_{tc} = F_{w(tc)} + F_{s(tc)} \text{ and } F_{d(tc)} + F_{s(tc)}, \tag{37}$$

where F_{tc} = Total net deposition flux on the tree canopy.

3. Results and discussion

3.1. Modelled NH_3 concentrations over Sri Lanka

The EMEP-WRF model has been extensively applied over the UK and Europe to estimate atmospheric NH_3 concentrations. Although this ACTM was originally developed and tested within Europe (Fagerli and Aas, 2008) and the UK (Vieno et al., 2009), its evaluation at a global scale by Ge et al. (2021) has enabled its global application. While modelled estimates of atmospheric NH_3 concentrations over Europe and the UK using the EMEP-WRF model are widely available, few studies have applied the model to other regions of the world. For example, Ellis et al. (2022) estimated NH_3 concentrations over the Himalayas and observed critical level exceedance over most of the region. In this study, its application over Sri Lanka reveals major NH_3 emission hotspots over urban and agricultural areas in the western and southern parts of the country (Fig. 6). Our hourly estimates over one year (2018) indicate south-westerly winds transporting this NH_3 towards the forested highlands in central Sri Lanka. This transport, however, is ephemeral and dependent on seasonal wind directions and emission patterns and results in high NH_3 concentrations over central Sri Lanka for brief periods (Fig. 6). Local sources in central Sri Lanka could also be partially contributing to these patterns.

3.2. Meteorological conditions

Although the Queensberry site in Sri Lanka has a higher altitude than Glencorse in Scotland, the conditions are nevertheless much warmer, representative of its tropical location (Fig. 7a). Mean monthly temperatures were 2–13 °C higher at Queensberry as compared to Glencorse, with lower difference observed in July and August. At both sites, the variation between above and below-canopy air temperature was minimal. On an average, above-canopy air temperature was 0.2 °C and 0.14 °C warmer at Glencorse and Queensberry, respectively. Higher temperatures can be expected to lead to higher compensation points, making the canopy and soils more susceptible to NH_3 emission.

At both sites, relative humidity is generally above 70%. Being a high-elevation sub-montane forest, the RH at Queensberry is generally higher except in the winter and rarely drops below 90% during the monsoons. Significant drops in RH (~60%) occur only during August in Glencorse and in November–December in Queensberry (Fig. 7b). Mean RH was 2.7% and 0.5% higher below the canopy at Glencorse and Queensberry, respectively. Overall higher RH at both sites is critical with respect to cuticular deposition as NH_3 dissolves more readily on water films that form on cuticular surfaces under humid conditions.

Above-canopy global solar radiation is larger at Queensberry (annual mean: 118 W m^{-2}) compared with Glencorse (annual mean: 94 W m^{-2}) reflective of the latitudinal differences. At Glencorse, 36% of the above-canopy radiation penetrates the canopy during winters, while only 18% penetrates during the growing season. In the evergreen forest in Queensberry, 32% above-canopy radiation penetrates the canopy annually. Global solar radiation at Glencorse shows a clear seasonal pattern with very low values during the winter months` (daytime monthly mean below canopy: 3.5 W m^{-2} in December), while at Queensberry, the reduction in solar radiation during winter is marginal as compared to the rest of the year. In-canopy solar radiation at both sites is generally similar until August, after which it remains consistently higher at Queensberry, due to a weaker diurnal variation in the winters as compared to the UK (Fig. 7c). Solar radiation is of particular importance in relation to stomatal deposition flux of NH_3.

Despite higher relative humidity at Queensberry, leaf wetness was lower with values between 38 and 73% as compared to Glencorse where leaf wetness was consistently above 90% throughout the study period. This difference is explainable because leaf wetness is not only driven by relative humidity but also air temperature, which contributes to the observed difference. As temperatures begin to drop in late-December in Sri Lanka, a sharp increase in leaf wetness is observed (Fig. 7d). Leaf wetness is an important parameter for modelling NH_3 dry deposition in some parameterisations as it drives the amount of NH_3 that can deposit on the epicuticular water film.

Soil temperature, which drives the soil compensation point, showed a strong seasonal pattern at Glencorse, while it remained generally consistent at Queensberry, with a gradual decrease autumn onwards (Fig. 7e). At both sites, mean monthly soil temperature was 0.3–1.8 °C lower than air temperature.

Both sites showed major seasonal differences in wind speed and wind direction. At Glencorse, wind speeds were highest in winter (Dec–Feb), associated with prevailing winds form the SW to NE, with SE winds more prevalent in other seasons (Fig. 8a). Wind speeds were generally lower at Queensberry, while wind direction was seasonally more variable with clear differences between monsoonal and inter-monsoonal periods (Fig. 8b).

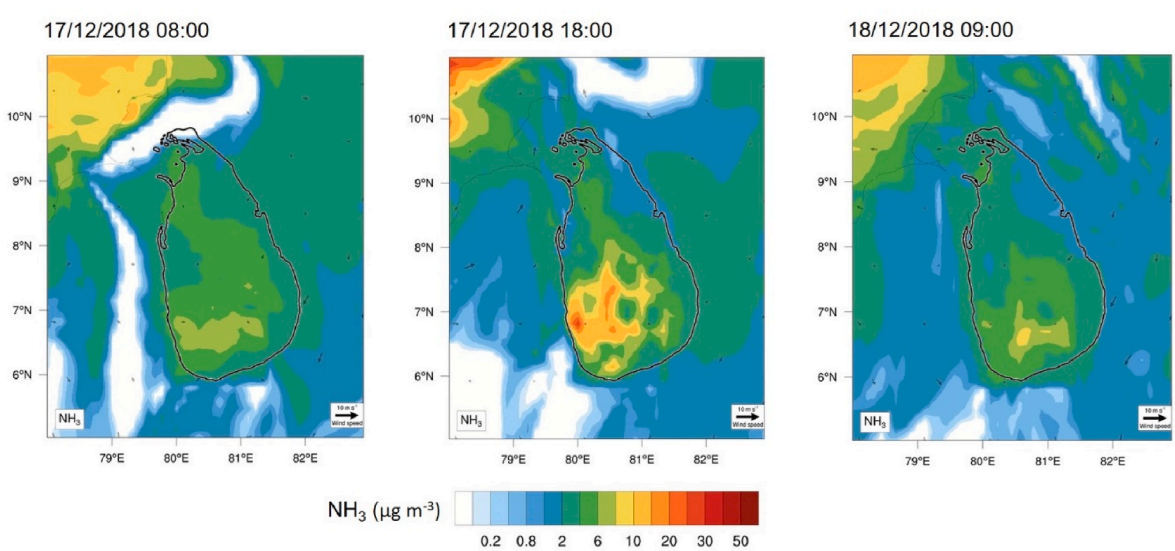

Fig. 6. One-hour atmospheric NH_3 concentration (μg m^{-3}) modelled using the EMEP-WRF model (0.11° x 0.11° resolution) on 17–18 December 2018.

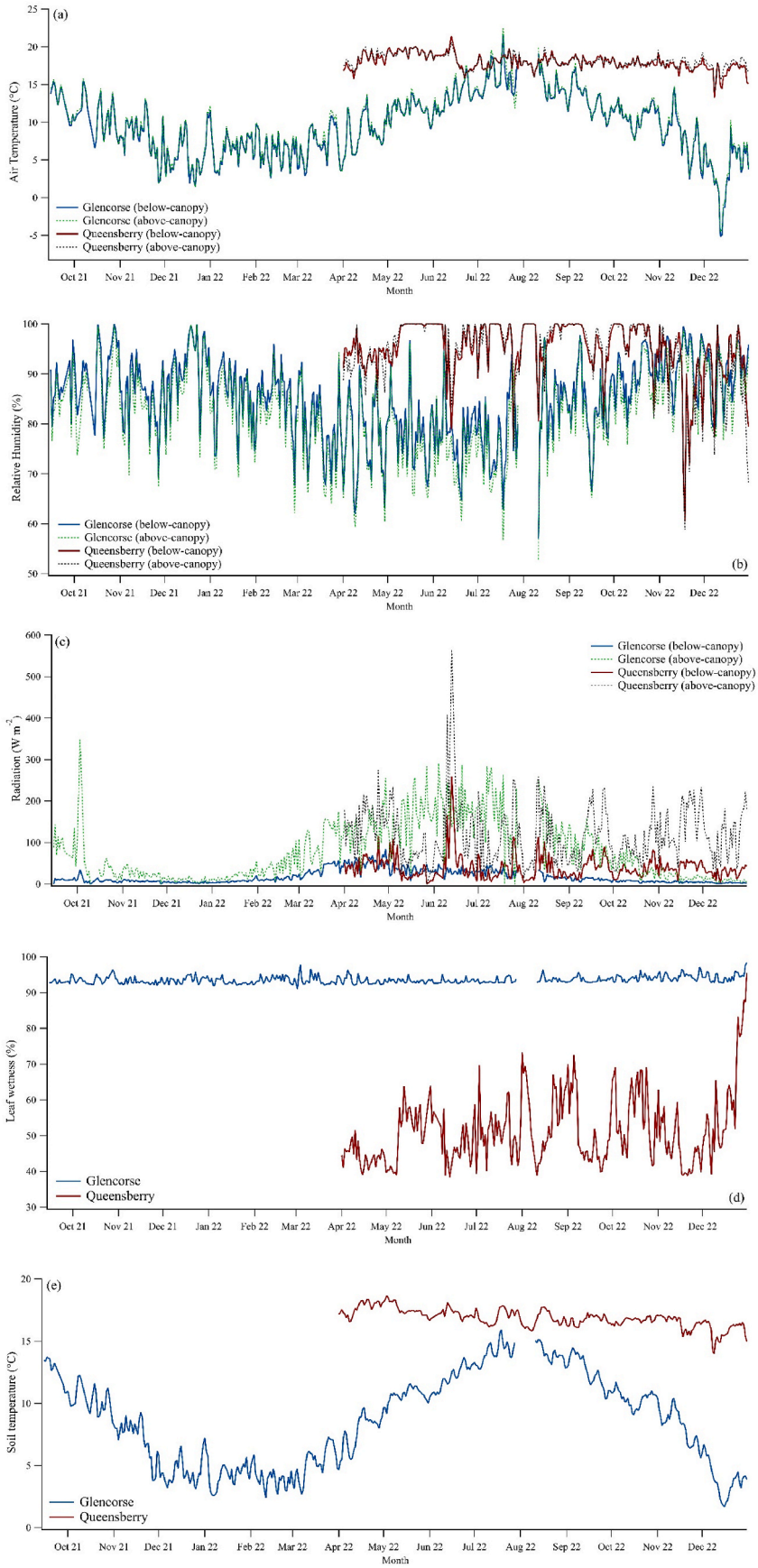

Fig. 7. Daily mean meteorological parameters measured above and below the canopy at both the sites. a) Air temperature (°C) b) Relative humidity (%) c) Global solar radiation (W m^{-2}) d) Below-canopy leaf wetness (%) and e) Soil temperature (°C) at 10 cm depth.

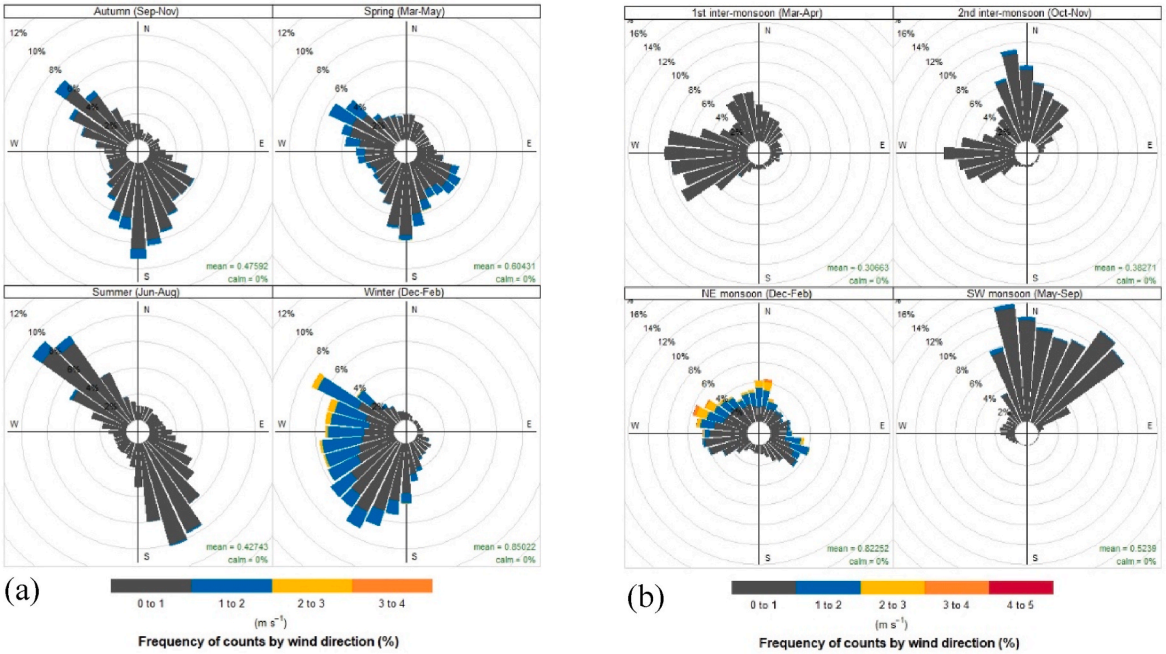

Fig. 8. Seasonal wind rose diagrams from a) Glencorse and b) Queensberry.

3.3. In-canopy air turbulence

Vertical profiling of wind parameters within and above the canopy is critical to understanding the vertical movement of a gas like NH_3. This profiling is even more critical in complex forest canopies and in situations where the emission source is located within the canopy. In this study, boundary layer resistances were calculated for four canopy layers including the soil surface, for which friction velocity (u^*) is an important parameter. The exchange of ammonia is determined by the level of turbulence, as characterised by u^* at different levels in the canopy. u^* controls boundary layer resistances, which decrease under higher wind speed (u). Vertical wind profiles have been studied across a range of different forest types with highly variable results (Lalic et al., 2003; Li et al., 2016; Moon et al., 2013, 2016; Oliver, 1971; Santana et al., 2017).

We observed significant differences in the u and u^* profiles between the Glencorse and Queensberry sites. Since vegetation surfaces play a major role in the wind movement within the canopy, profiles for summer periods with deciduous leaves (we term 'leaf-on' periods) and for winter periods without deciduous leaves (we term 'leaf-off' periods) in the Birch plantation varied significantly (Fig. 9a). At Glencorse, during the leaf-off period, wind speed increased rapidly from ground-level to the trunk space in the absence of a grass layer and followed a sigmoidal curve with minor variation between 3 and 12 m (top of the canopy). During the leaf-on period, however, wind speed was more variable with an abrupt increase at 7.35 m before decreasing at the top of the tree canopy.

This commonly observed 'secondary wind maximum' is attributed to winds moving relatively freely through the tree bole space which has a sparse structure (Shaw, 1977; Zeng and Takahashi, 2000). The associated increase in u^* (or the momentum flux) mid-canopy (Glencorse leaf-off) also suggests additional advection of air into the trunk space (Fig. 9b). At the Queensberry site, a generic wind speed profile was observed (Fig. 9a), in which wind speed remains consistent from ground vegetation layer up to the top of the tree canopy before increasing

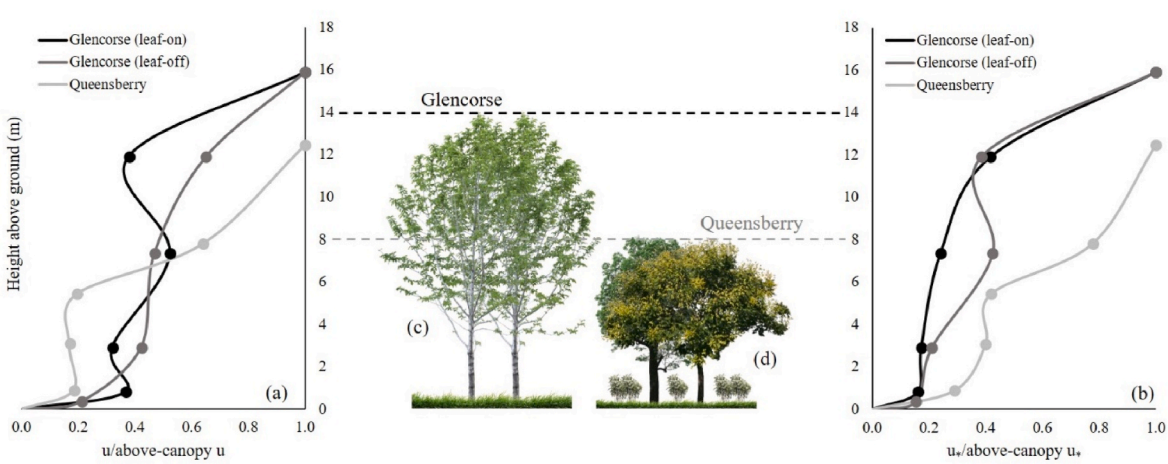

Fig. 9. Vertical profiles of (a) wind speed (u, m s^{-1}) and (b) friction velocity (u*, m s^{-1}) normalized by above-canopy measurements. Values are extrapolated to zero at the soil surface from the lowest measurement height above ground in the region not resolved by the measurements. Mean height (dashed lines) and canopy structure of the (c) Birch canopy at Glencorse and (d) tropical sub-montane forest in Queensberry are shown as reference. Measurement heights are shown as circles.

almost exponentially. This is the most commonly observed wind speed profile across forest types (Lalic et al., 2003; Oliver, 1971; Santana et al., 2017). A clear effect of a uniformly thick canopy structure with multiple layers of vegetation preventing wind penetration is evident from this profile (Fig. 9a).

3.4. Ammonia release

During the study period, the Glencorse release system was activated for 17% of the time, while the Queensberry system was activated for 31% of the time. This is mainly because of NH_3 release system operating for two wind directions, in order to account for the two monsoons and two inter-monsoon periods in Sri Lanka (Fig. 8b). Monthly release volume varied from 200 to 4800 standard litres at Glencorse and 1220–6700 standard litres at Queensberry. During most months, the system at Queensberry released more ammonia for longer periods (Fig. 10). The Glencorse system experienced minor technical problems in October 2021 and July 2022.

3.5. Gamma values and compensation points

The Gamma values for soil and leaf litter (Γ_g) varied significantly between the two sites. At Glencorse, a much lower value of 20 was obtained, while a significantly higher soil re-emission potential of the tropical soils was observed at Queensberry (Table 4). A higher re-emission potential results in higher compensation points and lower deposition rates. Mean soil pH was similar at both sites (5.3 and 5.6 at Glencorse and Queensberry, respectively), however, soil NH_4^+ concentration was much higher at Queensberry, resulting in a higher Γ_g of 520.

High NH_4^+ concentrations are often observed in tropical forest soils and can be attributed to a range of contributing factors such as high organic matter content (Gurmesa et al., 2022), warm and moist conditions (Neill et al., 1999), higher microbial activity (He et al., 2020; Xu et al., 2013), limited nitrification (Silver et al., 2001) and low NH_4^+ leaching rates (Silver et al., 2001). Very few estimates of Γ_g currently exist (Massad et al., 2010), out of which, most studies have been conducted in fertilized non-forest soils (David et al., 2009; Nemitz et al., 2000a, 2001; Walker et al., 2008). The Γ_g values estimated from these studies are high, ranging from 1500 to 104900. The only comparable estimate from non-fertilized forest soil was obtained by Walker et al. (2008). Their Γ_g value of 20 closely matches with Γ_g for Glencorse, while a higher Γ_g of 520 from Queensberry remains, to our knowledge, the only Γ_g estimate from a tropical forest.

Table 4
Γ values for soil and leaf litter layer and ground flora from both sites.

	$[H^+]$ (mol l^{-1})	$[NH_4^+]$ (mol l^{-1})	Γ
Glencorse soil and leaf litter	4.9×10^{-6}	9.6×10^{-5}	20
Glencorse understorey vegetation	–	–	1162
Glencorse tree canopy	–	–	1162
Queensberry soil and leaf litter	2.5×10^{-6}	1.3×10^{-3}	520
Queensberry understorey vegetation	–	–	542
Queensberry tree canopy	–	–	542

The Gamma values or apoplastic ratios for understorey vegetation (Γ_s) also varied significantly between the two sites, with the tropical understorey at Queensberry having a lower Γ_s than the grass-dominated understorey at Glencorse (Table 4). In absence of NH_3 and wind gradient measurements above both the forest canopies for AGM application, the same Γ_s values obtained for understorey vegetation were applied to the tree canopy. Apoplastic ratios were estimated within two months at Glencorse and two weeks at Queensberry from the start of the NH_3 enhancement experiments. While 3165 L of NH_3 had been released at Glencorse until the Γ_s estimation campaign, the Queensberry site was 'unfertilized' when Γ_s was estimated.

Our estimates are within the range of Γ_s values compiled by Massad et al. (2010) for unfertilized forests that range from 27 to 5604. Lowest values of Γ_s have been reported from Spruce (27–61) (Hartmann, 2005; Kesselmeier et al., 1993), rainforests (38.5) (Ramsay et al., 2021) and mixed Pine forest (141) (Langford and Fehsenfeld, 1992), followed by larger values from Beech (400) (Wang et al., 2011), mixed coniferous (1375–3300) (Neirynck and Ceulemans, 2008) and coniferous forests (5604) (Wyers and Erisman, 1998). In this study, the higher Γ_s value for the Glencorse Birch plantation can be attributed to two months of NH_3 exposure (fertilization) to the vegetation.

Both Γ_g and Γ_s values (and compensation points) at the two sites are expected to increase with time as the NH_3 enhancement experiments progress, resulting in lower net deposition rates in the future. As Γ values are known to be a variable and often an uncertain parameter in

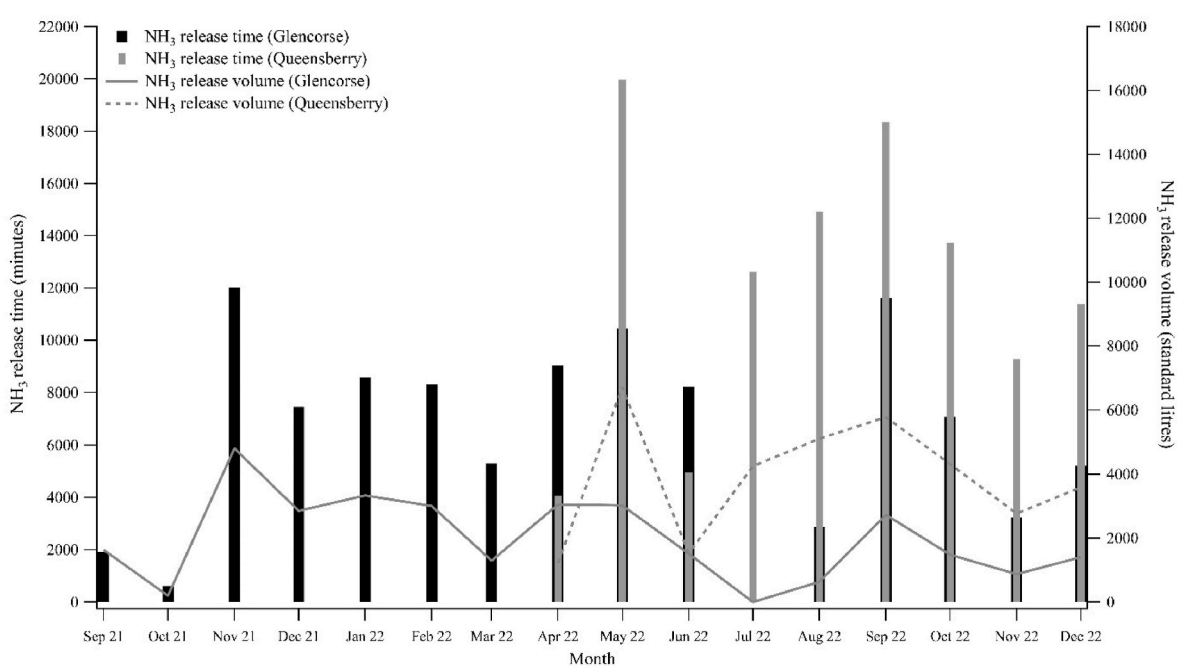

Fig. 10. Monthly NH_3 release times (minutes) and volumes (litres at standard atmospheric temperature and pressure) at both field sites.

deposition modelling (Hill et al., 2002; Loubet et al., 2002; Mattsson et al., 2009; Sutton et al., 2009a), a sensitivity analysis is provided in the supplementary material to show the effect of applying a wide range of Γ values on modelled NH_3 deposition rates.

Soil (χ_g) and stomatal (χ_s) compensation points provide insights on the switching of soils or vegetation from being sources to sinks of NH_3 and vice versa. Seasonal estimates of χ_g and χ_s from our sites provide an overview of the temporal trend of this NH_3 re-emission phenomenon. χ_g showed some seasonal variation at Glencorse with minimum values in winter (0.01 μg m^{-3}) and maximum values in mid-summer (0.04 μg m^{-3}) (Table 5). On the contrary, χ_g remained nearly constant throughout the year at Queensberry (0.05–0.06 μg m^{-3}) (Table 6), which can be attributed to similar temperatures across seasons in Sri Lanka in contrast to the UK. The slightly higher values of χ_g at Queensberry are a result of warmer temperatures and a higher Γ_g.

Mean monthly stomatal compensation points (χ_s) were higher than χ_g at both sites (1.01–3.05 μg m^{-3} at Glencorse and 1.42–2.07 μg m^{-3} at Queensberry) (Tables 5 and 6). At distances away from the source where NH_3 concentrations can be lower, χ_s at both sites can exceed NH_3 concentrations in the air, resulting in emission of NH_3 from the stomata. χ_s was not calculated for the leaf-off periods at Glencorse (November to February for the understory and November to March for tree canopy).

Foliar χ_s is known to be influenced by various biological and leaf metabolic factors such as root water and nutrient uptake (Mattsson and Schjoerring, 1996), NH_4^+ concentration in the xylem sap (Schjoerring et al., 2002), N assimilates in the phloem (Foyer et al., 2003), cell-apoplast exchange of NH_4^+ (Nielsen and Schjoerring, 1998), apoplastic pH (Pearson et al., 1998) and cellular NH_4^+ concentration (Leegood et al., 1995). χ_s in this study is a completely temperature-dependent parameter because Γ_s was kept constant throughout the study period and also along the transect.

3.6. Background ammonia concentrations and deposition

Background NH_3 concentrations indicate that both sites are relatively clean in terms of NH_3 pollution. Monthly background NH_3 concentrations at Glencorse increase in March and April (1.4 μg m^{-3}) before declining gradually (Fig. 11a). The spring increase can be attributed to regional manure spreading at this time, consistent with national observations. For example, Tang et al. (2018) observed a similar peak in April at a remote site in the Scottish Highlands. At our site, however, we did not record a second peak in July–August which is observed at many sites across the UK (Tang et al., 2018). Concentrations remained below 1 μg m^{-3} throughout the rest of the study period with very low concentrations measured during the winter months. The annual mean NH_3 concentration was 0.63 μg m^{-3}, which is below the international critical level of 1 μg m^{-3} for lichens and bryophytes.

Calculated net monthly background NH_3 dry deposition flux to Glencorse varied from 0.05 to 0.69 kg N ha^{-1} with a total annual flux of 2.3 kg N ha^{-1}. During winter (without leaves on deciduous trees) the dry deposition flux to the soil surface was dominant, while cuticular deposition to the understory was the most prominent flux during periods with deciduous leaves present, followed by cuticular deposition to the tree canopy (Fig. 11a). Throughout the period with leaves (Apr–Nov), leaf stomata remained an estimated net source of ammonia although monthly stomatal emission fluxes were low (0.0003–0.28 kg N ha^{-1}) (Fig. 11a), possibly because of the low background NH_3 concentrations and low solar radiation in Scotland, particularly within the forest canopy.

At Queensberry, monthly background NH_3 concentrations ranged from 0.03 to 1.02 μg m^{-3}, with a spike in October (Fig. 11b). Background concentrations remained below 1 μg m^{-3} with little seasonal variation for the rest of the study period (Fig. 11b) indicating a sufficient distance (0.4 km) from the fertilized tea plantations. The annual mean concentration was 0.35 μg m^{-3}.

Estimated total NH_3 fluxes from the vegetation layers dominated over the soil fluxes at Queensberry. Monthly estimated stomatal emission and cuticular deposition fluxes were nearly equal in magnitude resulting in small net flux ranging from −0.18 to 0.42 kg N ha^{-1} with deposition from July to October and net emission during the remaining months. Background knowledge of NH_3 emission sources, their relative contribution to atmospheric NH_3 and seasonal patterns of pollutant movement is relatively unknown in Sri Lanka. Our estimates provide baseline information on the status of NH_3 air concentrations and deposition over the forested highlands of central Sri Lanka, which can further help inform monitoring strategies and modelling estimates for tropical ecosystems.

It is critical to note that at both sites, annual background NH_3 concentrations are lower than UNECE NH_3 critical levels for lichens and bryophytes (annual average: 1 μg m^{-3}) and forest ground flora (annual average: 3 μg m^{-3}) (UNECE, 2007). Similarly, annual background NH_3 dry deposition of 1.3 kg N ha^{-1} at Glencorse and 0.34 kg N ha^{-1} at Queensberry to the understory layers is also below the total N_r critical load value for ground flora (10–15 kg N ha^{-1} yr^{-1}) (Bobbink et al., 2022). The NH_3 enhancement experiment is designed to simulate a wide gradient of NH_3 concentration and deposition values for comparison with current critical levels as a reference point. Therefore, the sites along with the monitoring experiments provide a reliable platform to understand and predict impacts on lichens, bryophytes and ground flora under very likely future scenarios of increased atmospheric NH_3 concentrations well above current critical levels (Cape et al., 2008; Franzaring and Kösler, 2022; Sutton et al., 2022). Low background concentrations observed at our sites reinforces their suitability for providing evidence of damage to non-vascular plants and fungi including lichens, and ground

Table 5
Mean monthly R (s m^{-1}) and χ (μg m^{-3}) values from Glencorse. Stomatal and cuticular resistances were set to infinite to simulate deposition during the leaf-off period.

Month	R_{bg}	$R_{b1(us)}$	$R_{b2(ts)}$	$R_{b3(tc)}$	$R_{s(us)}$	$R_{s(tc)}$	$R_{w(us)}$ Massad	$R_{w(us)}$ DEPAC	$R_{d(us)}$	$R_{w(tc)}$ Massad	$R_{w(tc)}$ DEPAC	$R_{d(tc)}$	χ_g	$\chi_{s(us)}$	$\chi_{s(tc)}$
Sep-21	246	144	1117	100	2781	2174	22	22	54	21	20	42	0.03	2.08	2.14
Oct-21	260	152	1160	105	3147	2460	13	14	22	10	1435	17	0.02	1.60	1.41
Nov-21	197	117	795	62	∞	∞	∞	∞	∞	∞	∞	∞	0.02	–	–
Dec-21	285	167	1022	88	∞	∞	∞	∞	∞	∞	∞	∞	0.01	–	–
Jan-22	182	108	756	57	∞	∞	∞	∞	∞	∞	∞	∞	0.01	–	–
Feb-22	144	87	647	46	∞	∞	∞	∞	∞	∞	∞	∞	0.01	–	–
Mar-22	280	164	1014	86	1794	∞	11	34	73	∞	∞	∞	0.01	1.01	–
Apr-22	260	152	956	80	1492	1461	14	47	94	14	57	92	0.02	1.23	1.23
May-22	221	130	1036	90	1332	1304	17	25	55	20	39	54	0.03	1.74	1.76
Jun-22	249	146	1128	101	1259	1232	22	22	57	28	39	55	0.03	2.16	2.23
Jul-22	238	140	1084	96	1887	1475	54	59	380	55	60	297	0.04	2.95	3.05
Aug-22	323	188	1352	130	2398	1875	40	51	503	39	48	393	0.04	2.54	2.60
Sep-22	256	150	1149	104	2765	2161	24	32	85	22	29	66	0.03	2.04	2.10
Oct-22	247	145	1124	100	3158	2469	13	14	22	13	14	17	0.02	1.55	1.60
Nov-22	352	205	1191	108	∞	∞	∞	∞	∞	∞	∞	∞	0.02	–	–
Dec-22	295	173	1056	91	∞	∞	∞	∞	∞	∞	∞	∞	0.01	–	–

Table 6
Mean monthly R (s m^{-1}) and χ (μg m^{-3}) values from Queensberry.

Month	R_{bg}	$R_{b1(us)}$	$R_{b2(ts)}$	$R_{b3(tc)}$	$R_{s(us)}$	$R_{s(tc)}$	$R_{w(us)}$ Massad	$R_{w(us)}$ DEPAC	$R_{d(us)}$	$R_{w(tc)}$ Massad	$R_{w(tc)}$ DEPAC	$R_{d(tc)}$	χ_g	$\chi_{s(us)}$	$\chi_{s(tc)}$
Mar-22	276	160	1002	85	2041	2500	10	1.33	1.84	13	2.05	2.25	0.06	1.42	1.43
Apr-22	268	157	964	83	1165	1427	16	1.85	4.18	25	4.2	5.12	0.06	1.76	1.87
May-22	98	61	595	42	1174	1437	16	1.4	2.95	21	2.37	3.61	0.06	2.01	2.07
Jun-22	94	58	575	40	1084	1328	12	1.41	2.37	18	3.07	2.9	0.06	1.61	1.7
Jul-22	110	67	622	46	1154	1413	13	1.43	2.67	20	3.29	3.27	0.05	1.71	1.8
Aug-22	224	151	1016	104	1149	1408	14	1.57	3.24	19	2.97	3.97	0.05	1.69	1.75
Sep-22	635	592	2696	409	1111	1360	14	1.67	3.43	20	3.4	4.21	0.05	1.75	1.81
Oct-22	212	193	1154	133	1166	1428	13	1.43	2.65	18	3.12	3.25	0.05	1.65	1.73
Nov-22	247	163	940	84	1149	1407	16	6.77	29.02	30	24	35.55	0.05	1.57	1.74
Dec-22	244	143	900	76	1184	1450	12	2.07	3.98	22	6.97	4.88	0.05	1.47	1.62

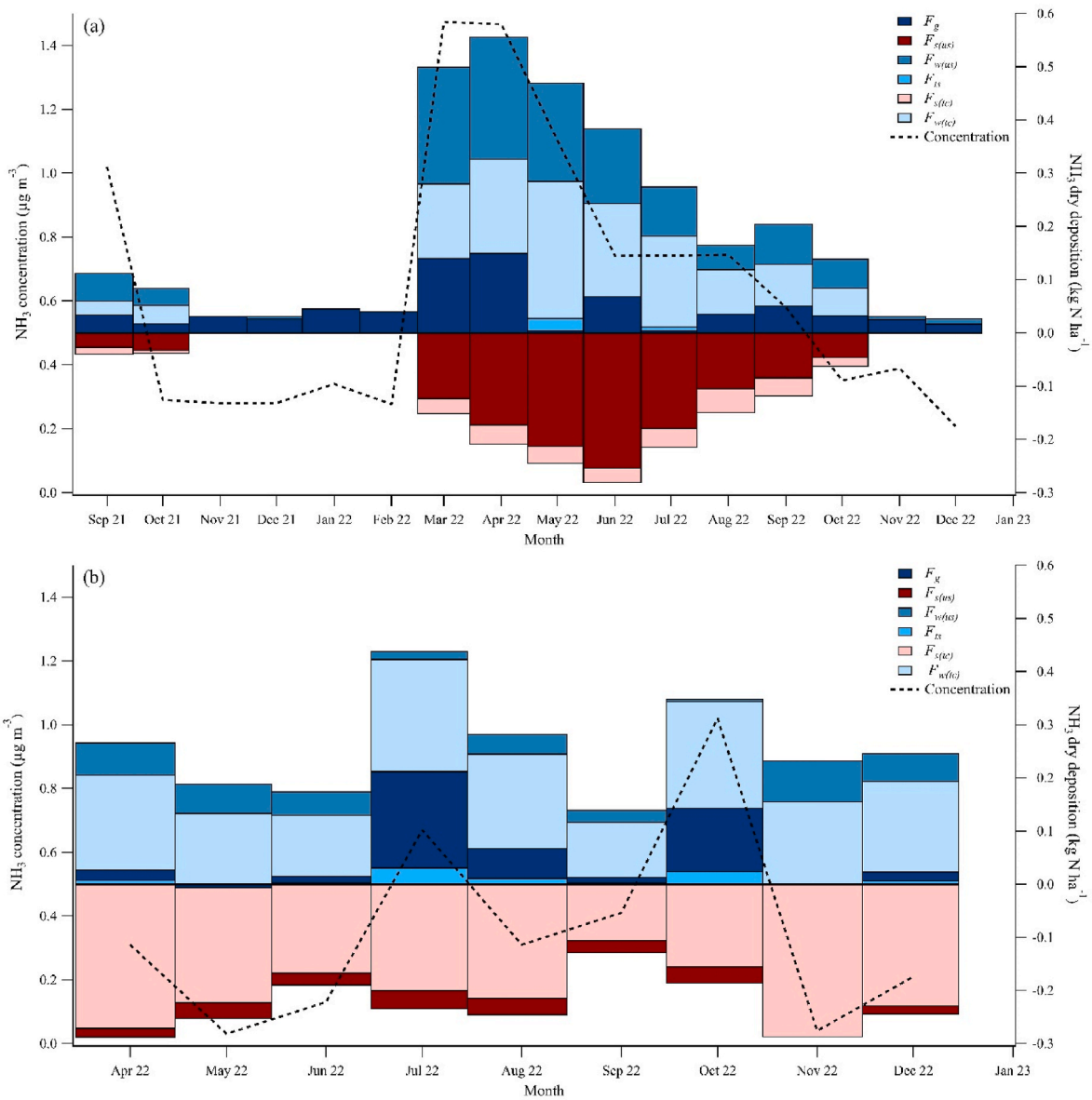

Fig. 11. Measured background NH_3 concentration (μg m^{-3}) and modelled background dry deposition (kg N ha^{-1}) to the different canopy layers at (a) Glencorse from September 2021 to December 2022 and (b) Queensberry from April to December 2022. F_w is estimated using the parameterisation given by Massad et al. (2010). Positive flux here indicates deposition and negative flux indicates emission.

flora to help establish new critical levels and loads for the regions (Franzaring et al., 2022).

3.7. NH_3 concentration gradients from the enhancement systems

Both the NH_3 enhancement systems generated logarithmically declining mean concentration gradients with distance away from the

source (Fig. 12), in line with theoretical expectation and previous enhancement studies such as Theobald et al. (2001), Leith et al. (2004) and Sheppard et al. (2011).

At Glencorse, concentrations ranged from 3.1 to 28.6 μg m^{-3} along the 44-m study transect ($y = -8.4\ln(x) + 33.5$, $R^2 = 0.99$), as compared with the background value of 0.63 μg m^{-3}. The bi-directional system at Queensberry generated higher concentrations along the south-western transect, responding to winds from the NE (mean 2.4–46.7 μg m^{-3}) ($y = -17.1\ln(x) + 62.3$, $R^2 = 0.98$), as compared with the north-eastern transect, responding to winds from the SW (mean 2.2–15.9 μg m^{-3}) ($y = -5.5\ln(x) + 19.7$, $R^2 = 0.99$) and the background value of 0.35 μg m^{-3}. Out of the total NH_3 release time at this site, the system released NH_3 towards the southwest for 69% of the time during the study period. A steeper gradient with higher concentrations and a gradual gradient with moderate concentrations provide a potential to study a wider range of NH_3 impacts.

Concentration ranges varied considerably from month-to-month depending on prevailing wind conditions. At Glencorse, the highest concentrations were recorded in November 2021 and lowest concentrations were recorded in January 2022. At Queensberry, highest concentrations were measured in May 2022 along the south-western transect and in December 2022 along the north-eastern transect. Lowest concentrations were measured in June 2022 along both transects. This intermittent and event-based release of NH_3 represents 'real-world' conditions while replicating NH_3 levels from common sources (Cape et al., 2004; Fowler et al., 1998; Groot Koerkamp et al., 1998; Manninen et al., 2023; Pitcairn et al., 1998; Tanner et al., 2022).

Vertical monitoring of NH_3 concentration at different time scales using ALPHA samplers (Fig. 13a) and the Picarro Analyser (Fig. 14a) at Glencorse indicated larger concentrations closer to the ground, especially around the grass layer, and a decrease with height. Similar vertical NH_3 gradients were observed by Theobald et al. (2001) inside a forest canopy. In the Birch plantation at Glencorse, a distinct trunk space with absence of foliar surfaces between the grass layer and lower tree canopy prevents mixing of the three plumes in air near the source. Stable stratification, typical for plant canopies, likely contributes to this effect. Concentrations increased downwards up to 25 cm from the ground but decreased at the soil surface (5 cm) (Fig. 13a). This could be due to a combination of factors such as NH_3 recapture by the grass layer and the soil boundary layer interfering with NH_3 diffusion into the samplers located at 5 cm from the ground.

At Queensberry, in the absence of a vertical array of ALPHA samplers, vertical NH_3 profiling was done using the Picarro NH_3 analyser with multiple inlets in combination with ALPHA samplers placed laterally along the monitoring transect. In contrast to Glencorse, better vertical mixing of NH_3 is clearly evident at Queensberry, as indicated by

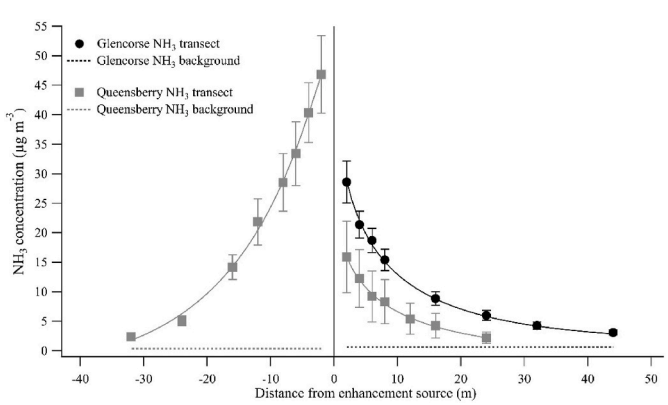

Fig. 12. Mean monthly NH_3 concentrations (μg m^{-3} ± SE) along the monitoring transect at Glencorse (black) and Queensberry (grey) measured using ALPHA samplers at 1.5 m from the ground. Background concentrations (dashed lines) are shown for reference.

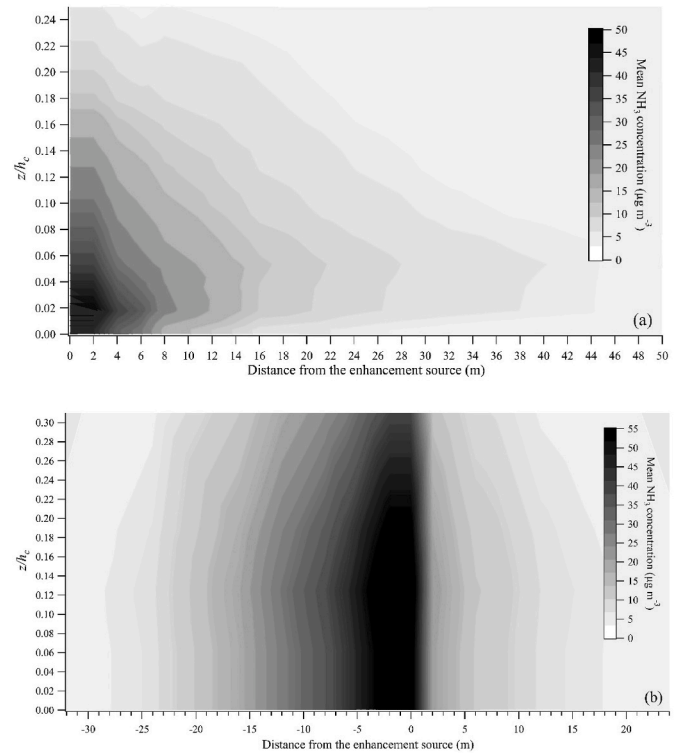

Fig. 13. Vertical and horizontal gradients of mean monthly NH_3 concentration (μg m^{-3}) measured a) at Glencorse (from vertical and lateral ALPHA measurements) and b) at Queensberry (from a combination of vertical Picarro and lateral ALPHA measurements). z/h_c is the measurement height (z) normalized by canopy height h_c.

more vertically uniform concentrations along both transects (Fig. 13b). This can be attributed to a dense canopy structure from the ground up to the tree canopy with fewer gaps and a less prominent trunk space, encouraging vertical rather than horizontal dispersion. Densely located foliar surfaces across all canopy layers promote the vertical mixing of eddies resulting in a uniform vertical NH_3 gradient. In contrast to Glencorse, upper layers of the tree canopy encounter similar NH_3 concentrations as the understory at Queensberry. A vertical NH_3 gradient becomes more prominent only at moderate (0.8–1.2 m s^{-1}) and high (1.2–10 m s^{-1}) wind speeds (Fig. 14b), which constitute only 13% of the total release time.

3.8. Resistances and NH_3 exchange fluxes

Applying the multi-layer resistance model allowed us to partition exchange fluxes including component deposition and emission fluxes across the canopy layers, when considering the fate of released NH_3. As shown by Figs. 15–18, at both field sites, the strongest sinks for NH_3 were the soil surface and leaf cuticles in the understory vegetation, followed by tree leaf cuticles and trunk surfaces. Leaf stomata in both understory and tree canopy were the weakest NH_3 sinks and even acted as NH_3 sources at the furthest distances away from the release system, where NH_3 concentrations were less than the estimated compensation points. Each of these canopy layers have different surface chemistry, moisture and biological response to meteorological conditions, which determines their ability to absorb NH_3 from the air (Nemitz et al., 2001). This characterization also helps locate the fate of the excess NH_3 and identify organisms that could be at risk of NH_3 impacts. The experimental enhancement provides a wide range of estimated NH_3 dry deposition to different parts of the canopy.

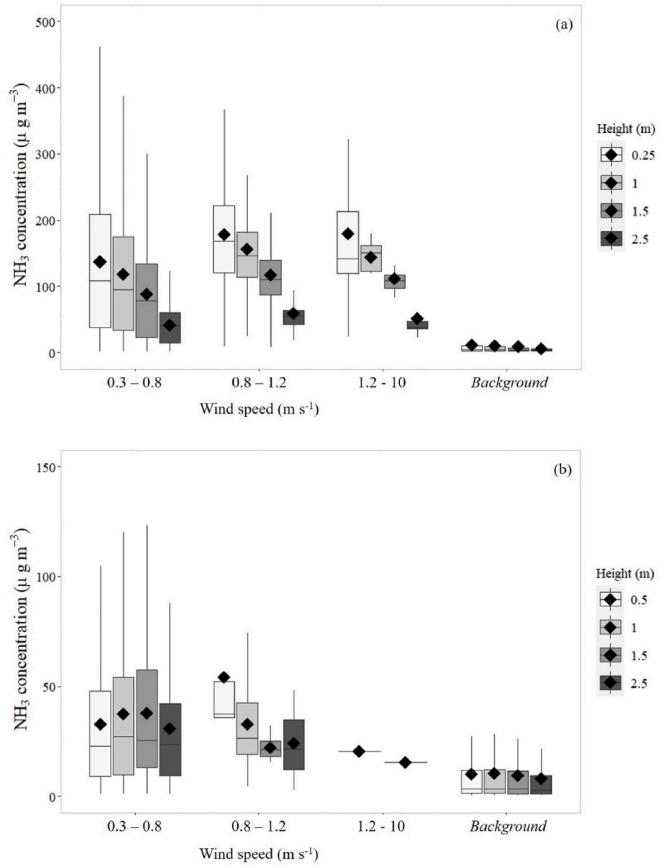

Fig. 14. NH_3 concentrations (μg m^{-3}) measured at four heights and 10 m away from the enhancement system using the Picarro analyser over 10-day campaigns at a) Glencorse and b) Queensberry. The background category shows measurements during no NH_3 enhancement irrespective of the wind speed. The box and whisker plots show the mean (diamond), median (central bar), interquartile range (box) and values within 1.5 times the interquartile range above and below 75th and 25th percentiles, respectively (whiskers).

3.8.1. NH_3 exchange with the soil surface

Monthly average quasi-laminar boundary layer resistance of the soil surface (R_{bg}) ranged between 144 and 352 s m^{-1} at Glencorse (Table 5) and was more variable at Queensberry (94–635 s m^{-1}) (Table 6). While a seasonal pattern emerged at Queensberry with lower R_{bg} during one of the monsoons, no seasonality was observed at Glencorse. Factors such as ground-level friction velocity and the temperature-dependent kinematic viscosity of air drive R_{bg} (Schuepp, 1977). Ground-level friction velocity, the strongest driver of R_{bg}, is derived from above-canopy friction velocity (Nemitz et al., 2000b). Therefore, the complex topography and pronounced fluctuations in seasonal wind conditions possibly explain the variability in R_{bg} at Queensberry.

At Glencorse, estimated deposition to the soil surface along the enhancement transect ranged from 3.6 to 71 kg N ha^{-1} yr^{-1} ($y = -22.2\ln(x) + 79.2$, $R^2 = 0.93$) as compared to a background F_g of 0.63 kg N ha^{-1} yr^{-1}. The two deposition gradients at Queensberry ranged from 1.7 to 95.6 kg N ha^{-1} yr^{-1} (SW of source) ($y = -36.3\ln(x) + 127.9$, $R^2 = 0.98$) and 1.1–27.5 kg N ha^{-1} yr^{-1} (NE of source) ($y = -10.8\ln(x) + 35.1$, $R^2 = 0.99$) (Fig. 15) as compared to a background F_g of −2.2 kg N ha^{-1} yr^{-1}.

Monthly variation in deposition rates was prominent due to seasonal effects on meteorology and varying NH_3 release rates from the source, simulating real-world deposition conditions. Because of the low soil compensation point and consistent NH_3 enhancement at Glencorse, the soil surface never acted as a net NH_3 source on a monthly scale. On the other hand, net NH_3 emission was observed during summer months

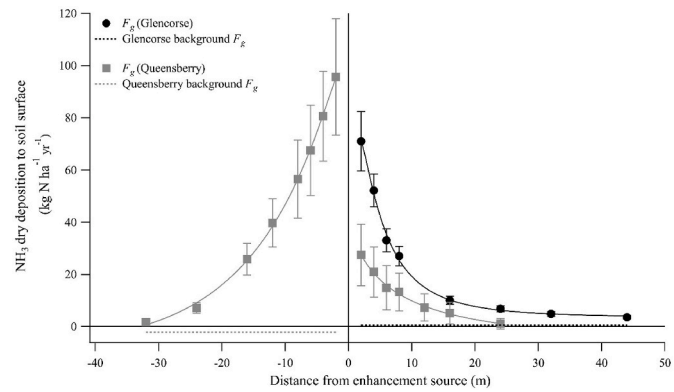

Fig. 15. Gradients of NH_3 exchange (kg N ha-yr^{-1} ± SE) with the soil surface at both sites. Dashed lines indicate background NH_3 flux at the soil surface for reference.

along the NE transect at Queensberry because of lower NH_3 release in this direction. Thresholds for impacts of NH_3 deposition on soils are variable depending on soil and vegetation type; however, elevated deposition conditions created at both sites are likely to induce varying degrees of negative effects in the soil. These are likely to include higher N_2O emissions (Leeson et al., 2017), changes in soil chemistry (especially pH) (Dise et al., 2011), decline in microbial diversity (Ma et al., 2022) and loss of non-vascular plants and fungi including lichen species growing on the ground (Sheppard et al., 2011).

3.8.2. NH_3 deposition flux to trunk surfaces

Deposition flux to the trunk surface layer was one of the smallest fluxes estimated from the resistance model. At Glencorse, NH_3 deposition to the trunk surfaces ranged from 0.9 to 8 kg N ha^{-1} yr^{-1} ($y = -2.4\ln(x) + 9.4$, $R^2 = 0.98$) with a background flux of 0.1 kg N ha^{-1} yr^{-1}. At Queensberry, deposition to the trunk surfaces along the SW transect ranged from 0.8 to 17 kg N ha^{-1} yr^{-1} ($y = -6.4\ln(x) + 23.2$, $R^2 = 0.98$) and 0.8–6 kg N ha^{-1} yr^{-1} along the NE transect ($y = -2.1\ln(x) + 7.3$, $R^2 = 0.99$), as compared to a background F_{ts} of 0.1 kg N ha^{-1} yr^{-1} (Fig. 16). It is, however, unclear if these fluxes are enough to cause long-term changes in bark pH. The presence of lichens and bryophytes on tree trunks and their gradual change due to NH_3 exposure is expected to affect the boundary-layer and also needs to be further investigated.

Although parameterisations for R_b over leaf and soil surfaces are commonly used, R_b over tree trunks is difficult to formulate and rarely applied. Instead of diffusing and getting assimilated, gas molecules 'bounce-off' woody and bluff surfaces like tree trunks (Chamberlain et al., 1984), which explains higher R_b ($R_{b(ts)}$) values for the trunk

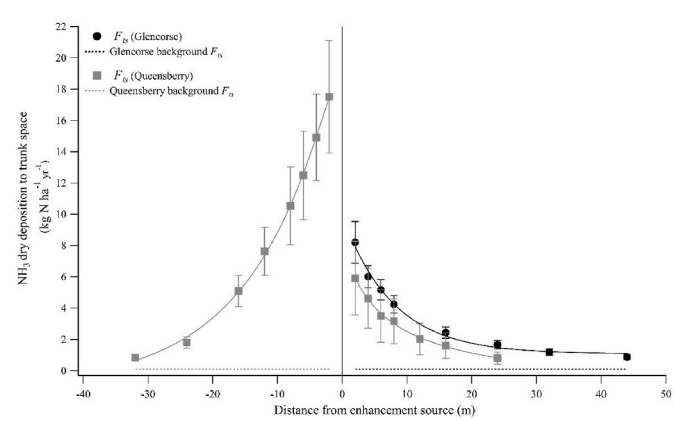

Fig. 16. Gradients of NH_3 deposition (kg N ha-yr^{-1} ± SE) to the trunk surfaces at both sites. Dashed lines indicate background NH_3 deposition to trunk surfaces for reference.

surfaces than for soil and vegetation. NH_3 dry deposition to tree trunks is of particular importance to this study because one of our long-term objectives is to monitor NH_3 deposition impacts on corticolous lichens and bryophytes. NH_3 deposition can gradually increase bark pH and subsequently impact lichen health and growth (van Herk, 2001; Wolseley et al., 2006). However, in this study, since high $R_{b(ts)}$ values result in low deposition flux on trunk surfaces, lichens are likely to be initially affected more severely by absorption of toxic NH_3 concentrations from the air than by changes in bark pH. Estimation of direct NH_3 deposition to lichens and bryophytes needs additional measurements and parameterisation, which will be further investigated as NH_3 exposure continues and bark pH changes.

3.8.3. NH_3 exchange with vegetation

Quasi-laminar boundary layer that forms over soil and vegetation surfaces can be a major source of resistance to NH_3 dry deposition (Sutton et al., 1993a). Gas molecules have to diffuse through this additional layer while getting transferred from the air to the surface. Boundary layer resistances (R_b) are strongly dependent on wind speed and friction velocity but also influenced by molecular diffusivity of the pollutant gas, kinematic viscosity of air at a given temperature, and roughness length (Fowler and Unsworth, 1979; Wesely et al., 1985). Boundary layer thickness generally diminishes under unstable conditions (high wind speeds), thereby increasing the deposition velocity. R_b around leaf surfaces is a critical parameter in this study since NH_3 is released from within the canopy. Monthly R_b values around varied from 46 to 205 s m^{-1} at Glencorse and 40–592 s m^{-1} at Queensberry. Boundary layer resistances over leaf surfaces did not show a strong seasonal trend at either site but at Queensberry, all R_b values peaked in September, which is possibly due to shifting monsoonal conditions, especially wind (Table 6, Fig. 8b).

3.8.3.1. NH_3 deposition flux to leaf cuticles and model performances.

Cuticular deposition (F_w) was dominant in both vegetation layers, however, estimates obtained using four different parameterisation yielded considerable differences.

3.8.3.1.1. NH_3 concentration-dependent parameterisation from Jones et al. (2007a). Cuticular deposition estimated using the NH_3 concentration-dependent parameterisation for moorlands from Jones et al. (2007a) was the lowest at high NH_3 concentrations near the source (<16 m) at both sites (Fig. 17a and b). In the NE transect at Queensberry, where NH_3 enhancement is the lowest, F_w modelled using this parameterisation was similar to F_w estimated using Massad et al. and the capacitance models. A similar trend was observed at Glencorse and the SW transect at Queensberry with decrease in NH_3 concentrations away from the source. The decrease in understorey F_w with distance from the source was linear, ranging from 7 to 10 kg N ha^{-1} yr^{-1} at Glencorse ($y = -0.06x + 10.2$, $R^2 = 0.99$) (Figs. 17a), 24–35 kg N ha^{-1} yr^{-1} along the SW transect at Queensberry ($y = -0.36x + 36.6$, $R^2 = 0.95$) and 20–26 kg N ha^{-1} yr^{-1} along the NE transect ($y = -0.27x + 26.2$, $R^2 = 0.88$) (Fig. 17b). In the tree canopy, similar trends were observed but with 30–60 % higher F_w as compared to the understorey layer at both sites, mainly driven by higher above-canopy solar radiation.

The concentration dependency in this parameterisation is meant to reflect saturation towards uptake at high concentrations, conceptually similar to the capacitance and DEPAC methods. However, it is to be noted that the linear relationship between R_w and NH_3 concentration observed by Jones et al. (2007a) was derived for a complex structured moorland vegetation canopy. The NH_3 concentrations were much higher (up to 100 μg m^{-3}) than in this study (up to 47 μg m^{-3}), which possibly constraints F_w estimation at high NH_3 concentrations using this parameterisation in our woodland study.

3.8.3.1.2. Temperature, RH and LAI-dependent parameterisation from Massad et al. (2010). Cuticular deposition to the understorey vegetation estimated using the RH-dependent parameterisation of R_w derived by

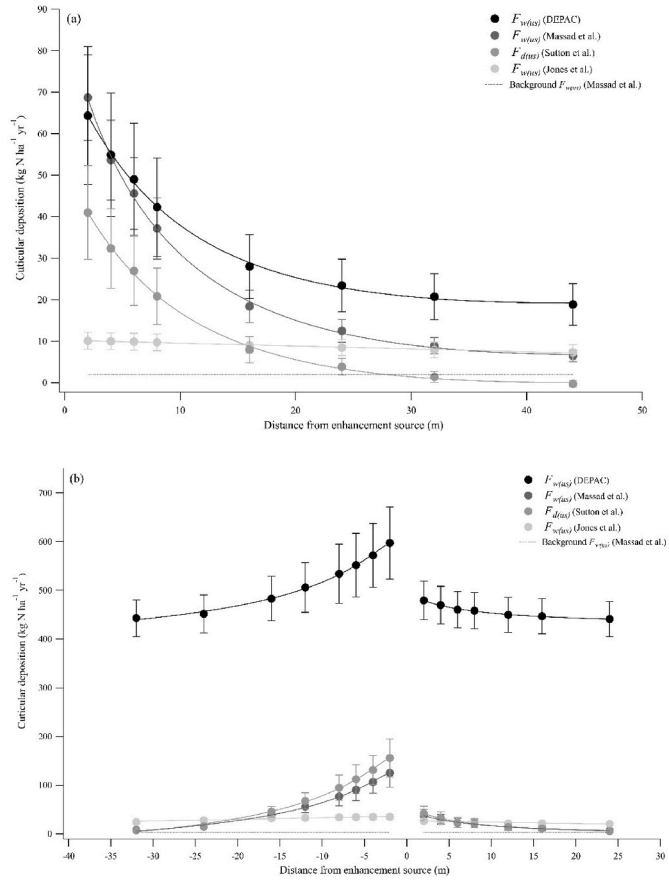

Fig. 17. Cuticular deposition to the understory ($F_{w(us)}$, kg N ha^{-1} yr^{-1} ± SE) estimated using four different parameterizations along the NH_3 gradients at (a) Glencorse and (b) Queensberry. dotted lines indicate mean background $F_{w(us)}$.

Massad et al. (2010) ranged from 6 to 69 kg N ha^{-1} yr^{-1} at Glencorse ($y = -21.2\ln(x) + 82.3$, $R^2 = 0.98$). At Queensberry, understorey F_w ranged from 8 to 125 kg N ha^{-1} yr^{-1} along the SW transect ($y = -45.2\ln(x) + 165.8$, $R^2 = 0.98$) and 7–37 kg N ha^{-1} yr^{-1} along the NE transect ($y = -12.5\ln(x) + 46.2$, $R^2 = 0.99$). In the tree canopy, F_w was significantly lower than in the understorey at Glencorse (59–84%). Contrastingly, at Queensberry, F_w in the tree canopy was 10–40 % higher than in the understorey.

This parameterisation adds temperature and LAI dependency to the commonly used RH-dependent parameterisation from Sutton et al. (1993). Temperature and RH dependency provides a comprehensive relationship between R_w and environmental conditions, while LAI dependency improves R_w estimation under varying phenological and seasonal conditions.

3.8.3.1.3. Leaf surface NH_3 concentration-dependent parameterisation from the DEPAC module (van Zanten et al., 2010). DEPAC parameterisation showed clear differences than the other parameterisations by estimating much higher F_w at both sites (Fig. 17a and b). However, close to the source (<6 m) at Glencorse, understorey F_w from the DEPAC parameterisation was similar to that from Massad et al. (Fig. 17a). At Queensberry, increasing with distance from the source, the DEPAC parameterisation estimated understorey F_w 5–140 times higher than Massad et al.'s parameterisation, 15–23 times higher than Jones et al.'s parameterisation and 4–480 times higher than the capacitance model in the understory layer (Fig. 17b). Understorey F_w ranged from 19 to 64 kg N ha^{-1} yr^{-1} at Glencorse ($y = -15.8\ln(x) + 75.6$, $R^2 = 0.98$), 443–597 kg N ha^{-1} yr^{-1} along the SW transect ($y = -59.6\ln(x) + 650$, $R^2 = 0.98$) and 441–479 kg N ha^{-1} yr^{-1} along the NE transect ($y = -15.7\ln(x) + 490$, $R^2 = 0.99$) at Queensberry. In the tree canopy, estimated F_w was

5–62 % lower at Glencorse and 16–36 % lower at Queensberry as compared to the understorey layer, driven by lower RH in the upper tree canopy.

Although it accounts for cuticular NH_3 re-emission which reduces F_w and has a similar core principle of RH-dependency as Massad et al.'s parameterisation, DEPAC overestimates F_w for these sites. This is possibly caused by the LAI-scaling parameter which is related to the LAI measured at the Haarweg site (van Zanten et al., 2010). The Haarweg site is dominated with perennial ryegrass, with LAI and canopy structure very different from forest sites. The LAI-scaling parameter in the DEPAC module, therefore, needs to be applied with caution to forest canopies.

3.8.3.1.4. Capacitance model from Sutton et al. (1998a). The capacitance model was the only one that estimated net cuticular emission at low NH_3 concentrations farther away from the NH_3 source at Glencorse (Fig. 17a), but not at Queensberry (Fig. 17b). Understorey F_d rates ranged from −0.2 to 41 kg N ha^{-1} yr^{-1} at Glencorse ($y = -14.3\ln(x) + 51.1$, $R^2 = 0.98$), 7–156 kg N ha^{-1} yr^{-1} along the SW transect ($y = -57.3\ln(x) + 207$, $R^2 = 0.98$) and 5–42 kg N ha^{-1} yr^{-1} along the NE transect ($y = -15\ln(x) + 52.4$, $R^2 = 0.99$) at Queensberry. At Glencorse, deposition to the tree leaf cuticles was much lower than to the understorey vegetation. Net cuticular deposition in the tree canopy occurred only up to a distance of 8 m from the source at a rate of 0.5–2 kg N ha^{-1} yr^{-1}. At Queensberry, F_d in the understorey and tree canopy were similar farther from the source but 43% higher in the tree canopy near the source.

This model takes into account previously deposited NH_3 and the thickness of the water film on cuticles. At Queensberry, where the conditions are tropical, the cuticular water film thickness was found to be consistently higher than at Glencorse (supplementary material), allowing for more cuticular deposition of NH_3.

3.8.3.2. NH_3 exchange with leaf stomata. Stomatal deposition was generally the smallest flux at both sites (Fig. 18). Net stomatal emissions were commonly observed at Glencorse and along the NE transect at Queensberry. At Glencorse, stomatal emissions occurred beyond 16 m from the enhancement system in the understory resulting in a gradient of −0.5 to 3.3 kg N ha^{-1} yr^{-1} along the transect ($y = -1.3\ln(x) + 4.2$, $R^2 = 0.98$), while the tree stomata were a constant NH_3 source (−0.8 to −0.2 kg N ha^{-1} yr^{-1}) ($y = -0.01x - 0.2$, $R^2 = 0.91$) (Fig. 18). At Queensberry, higher stomatal deposition ranging from −2 to 11 kg N ha^{-1} yr^{-1} in the understory ($y = -5.1\ln(x) + 15.7$, $R^2 = 0.98$) and −1.6 to 18.2 kg N ha^{-1} yr^{-1} in the tree canopy ($y = -7.7\ln(x) + 25$, $R^2 = 0.98$) was observed along the SW transect (Fig. 18). In comparison, along the NE transect, only −2.2 to 1.9 kg N ha^{-1} yr^{-1} stomatal deposition was estimated in the understory ($y = -1.6\ln(x) + 3$, $R^2 = 0.99$) and −1.4 to 6 kg N ha^{-1} yr^{-1} in the tree canopy ($y = -3\ln(x) + 8.1$, $R^2 = 0.99$), as a result of lower NH_3 concentrations along the NE transect (Fig. 18). In contrast to Glencorse, stomatal deposition to the tree canopy was estimated to be higher than in the understory at Queensberry.

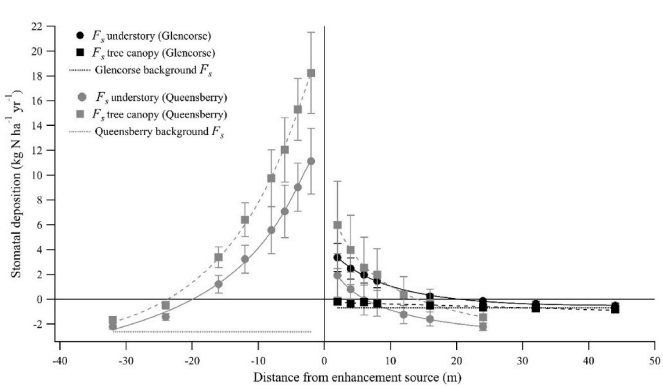

Fig. 18. Stomatal deposition (F_s) on the two vegetation layers (kg N ha^{-1} yr^{-1} ± SE) along the NH_3 transects at Glencorse (black) and Queensberry (grey). Circles and solid lines indicate the understory layer, squares and dashed lines indicate tree canopy and dotted lines indicate mean background F_s.

Although the tree canopy receives more solar radiation, which drives NH_3 deposition to the stomata, stomatal emission from the trees at Glencorse can possibly be explained by the strong vertical gradient in NH_3 concentrations resulting in much lower NH_3 concentrations in the tree canopy. Contrastingly, at Queensberry, where vertical NH_3 concentrations have minimal variation, higher stomatal deposition was estimated in the tree canopy than in the understory, mainly driven by above-canopy solar radiation. NH_3 emissions from the stomata are strongly driven by stomatal emission potential (Hansen et al., 2017), which is much higher for vegetation at Glencorse in this model. Additionally, lower F_s at Glencorse can partially be a result of relatively low radiation levels within the canopy and generally high cloud cover between September and March.

The exceedance of F_s over F_w at high NH_3 concentration has been proposed (Sutton et al., 1993a, 1993b) and shown to be true for moorland plants (Jones et al., 2007b). In this study, however, we did not observe this crossover at a monthly time scale, which suggests the possibility of lower cuticular NH_3 saturation in forest vegetation. The dominance of cuticular deposition over stomatal deposition also indicates possible recapture of NH_3 emitted by the stomata into leaf cuticles (Neirynck and Ceulemans, 2008; Nemitz et al., 2004).

3.9. Uncertainties in the deposition estimates

Modelling NH_3 dry deposition using the resistance method involves complexities that are related to a large number of measurements, parameterisations and assumptions (Massad et al., 2010). Therefore, some uncertainties need to be acknowledged despite making all efforts to minimise them. In this study, we used monthly mean NH_3 concentrations to drive the deposition model. Although this provides adequate estimates of deposition over a monthly time-scale, NH_3 concentration measurements at a higher temporal resolution are warranted to detect ephemeral changes in the flux, which can sometimes be significant. To calculate cuticular deposition using the capacitance model, we assumed a constant leaf pH. However, a more dynamic approach of using variable leaf pH would further improve the estimation of cuticular deposition. Γ values are known to vary seasonally and with NH_3 deposition over time (Hill et al., 2002; Loubet et al., 2002; Mattsson et al., 2009; Sutton et al., 2009a). However, we used constant Γ values throughout the study period and across our NH_3 concentration gradients. A concerted effort to estimate seasonal Γ values either by extraction or micrometeorologically along the NH_3 gradients would constrain the uncertainty in this model, but would be labour and resource intensive. Moreover, added instrumentation to estimate NH_3 concentrations at multiple heights above the tree canopy would enable the estimation of Γ_s for trees. Ideally, the AGM should be applied using multiple analysers measuring NH_3 concentrations simultaneously. This being an expensive method, Kamp et al. (2020) assessed the effect of using a single analyser with non-simultaneous measurements switching between heights (a method used in this study) and calculated an error of less than 7% in this technique.

To bring about the next step-change in deposition modelling, the resistance method needs to be applied in tandem with improved technologies. For example, LAI, LAD and the areas of different surfaces within each canopy layer can be accurately measured using ground-based Lidar, which can then be incorporated into deposition models at least at the site scale. Secondly, using multiple high-resolution NH_3 analysers to simultaneously measure NH_3 concentrations at different distances away from the source and at multiple heights within the canopy can further improve our understanding of the movement and behaviour of NH_3 within canopies. A campaign study to isotopically label the released NH_3 and analysing plant tissues and soil for $\delta^{15}N$ can provide a direct verification of deposition modelling parameters, although this method can be expensive and would require destructive

sampling.

3.10. Representativeness and implications for NH_3 impacts assessment

Both study sites experienced background NH_3 concentrations lower than the NH_3 critical level prior to the controlled NH_3 enhancement. This makes them well-suited for long-term assessment of the NH_3 critical level for woodland ecosystems and the specific plant groups present. The concentration gradients and estimated deposition rates represent a range of enhanced NH_3 conditions observed in the vicinity of sources such as poultry farms (Fowler et al., 1998; Pitcairn et al., 1998), livestock units (Groot Koerkamp et al., 1998; Pitcairn et al., 1998) and agricultural fields (Tanner et al., 2022). The elevated NH_3 concentrations and deposition rates at both sites are likely to induce negative environmental effects such as higher soil N_2O emissions, changes in soil chemistry, decline in soil microbial diversity, changes in abundance and species composition of grasses, non-vascular plants and fungi including lichens. To monitor these effects, we have established impact assessment studies at both sites. These include chambers to measure soil emissions, sampling points for chemical analysis of soil, permanent monitoring quadrats to study effects on lichens, bryophytes, fungi and ground flora and trees marked for measuring changes in bark pH along the NH_3 transects. Moreover, as mosses and lichens are sensitive bio-indicators of NH_3 pollution, time-lapse cameras pointing at mosses and lichens have been set up to visualize any morphological damage along the NH_3 transects. This monitoring setup in combination with the enhancement system and meteorological tower provides an ideal platform to assess and revise critical levels and loads for forest species, especially in South Asia, where such thresholds are not yet quantified (Franzaring and Kösler, 2022).

In addition to being bioindicators, sensitive organisms such as lichens are important non-timber forest products in high elevation areas of South Asia and economically beneficial to a large number of people (Chatterjee et al., 2017). Loss of such organisms due to NH_3 pollution can have adverse socio-economic impacts on local communities. The biological impacts – the point at which these species experience damage – therefore, need to be demonstrated more clearly to bring about effective policy changes (Ellis et al., 2022).

In the UK and European Union, critical levels (CLEs) of atmospheric NH_3 concentrations and critical loads (CLOs) of N deposition have been determined, above which harmful ecological effects have been demonstrated. Timely revision of critical levels and loads and continuous monitoring of their exceedances is needed to enable swift policy-related and actionable response (Sutton et al., 2022). Setting critical levels and loads is one of the first steps towards delivery of effective policy, though these thresholds are absent in tropical and south Asian ecosystems. For example, the CLE values for NH_3 agreed by the UN Economic Commission for Europe (UNECE, 2007) are based entirely on European data. For ecosystems where lichens and bryophytes are important for ecosystem integrity, the annual CLE is set at 1 μg m^{-3}, which is exceeded in about 69% of land area of the UK; the equivalent CLE value for higher plants including forest ground flora is 3 μg m^{-3}, which is exceeded across 6.3% of land area (Rowe et al., 2022). Application of annual CLEs for lichens and bryophytes to sub-Himalayan forests showed exceedance in 80–85% land area, while noting the need for more underpinning evidence (Ellis et al., 2022). In addition to annual CLE values, CLEs have also been set for hourly, daily and monthly periods at 3300, 270 and 23 μg m^{-3}, respectively (UNECE, 2007).

While CLEs are determined for species guilds and vegetation types (Franzaring and Kösler, 2022; Posthumus, 1988), empirical values for CLOs are established for ecosystem types and range from 3 to 20 kg N ha^{-1} yr^{-1} for different forest habitats (Bobbink et al., 2022). In the UK, CLOs are currently exceeded over more than 80% of the area for seven sensitive habitats including most woodland types (Rowe et al., 2022), whereas the application of the same CLO values to sub-Himalayan forests shows exceedance in 95–98% area (Ellis et al., 2022).

Ground flora, non-vascular plants, lichens and fungi are expected to have significant variation in their tolerance threshold to air pollutants (CLEs and CLOs) depending on factors such as climate, biogeography and historic exposure to pollution. For example, UK and EU CLEs and CLOs may not apply to South Asian ecosystems. It is therefore critical to determine thresholds at regional scale by studying dose-response relationships under natural conditions in specific ecoregions. In the UK and EU, CLEs and CLOs have been agreed by the United Nations Economic Commission for Europe (UNECE) under the Convention on Long-Range Transboundary Air Pollution (Sutton et al., 2009b), with these being used as part of the Gothenburg protocol to control transboundary air pollution. The CLE and CLO values are also used in planning assessments as part of national or international habitat protection, such as of the EU Habitats Directive. A similar process must be replicated in other regions of the globe where sensitive ecosystems are under a threat from air pollution. These thresholds, when incorporated into national environmental policies, place a legal requirement for development projects to maintain pollutant levels below the thresholds in the affected area. The effectiveness of these policies must be tracked through regular environmental impact assessments and audits. Additionally, once regionally appropriate CLEs and CLOs are determined, the evidence provided by field enhancement studies over time needs to be used to update CLE and CLO values. The UK and EU CLEs and CLOs for NH_3 were reviewed in 2022 and were retained at the current values (Franzaring et al., 2022).

A significant amount of NH_3 released from the enhancement systems was dry deposited within the study areas (Fig. 19). 26% and 64% of the released NH_3 deposited within the study plot at Glencorse and Queensberry, respectively. These estimates are higher than previous studies that observed 8–16% of NH_3 depositing within the first 300–500 m from livestock sources (Fowler et al., 1998; Hao et al., 2006; Shen et al., 2018; Walker et al., 2008; Yi et al., 2021). However, some modelling studies have estimated higher deposition rates of up to 60% in proximity of NH_3 sources (Asman, 1998; Sutton et al., 1998b), while Yi et al. (2020) found that 80% of the NH_3 released from a paddy field deposited within the first 100 m. The higher deposition/emission ratios observed in our study can be attributed to the location of the enhancement systems being inside the undisturbed forest canopy, including zero vegetation clearance during experimental construction to maintain a natural vegetation canopy structure. Much higher deposition in the tropical forest at Queensberry as compared to temperate Glencorse can be explained by higher tree density and LAI, which provide more surface area for the NH_3 to deposit. Additionally, Queensberry is an evergreen forest, while the deciduous Glencorse loses foliage for four months during winter, resulting in negligible stomatal and cuticular deposition during this period.

Several studies have been conducted to estimate NH_3 deposition over

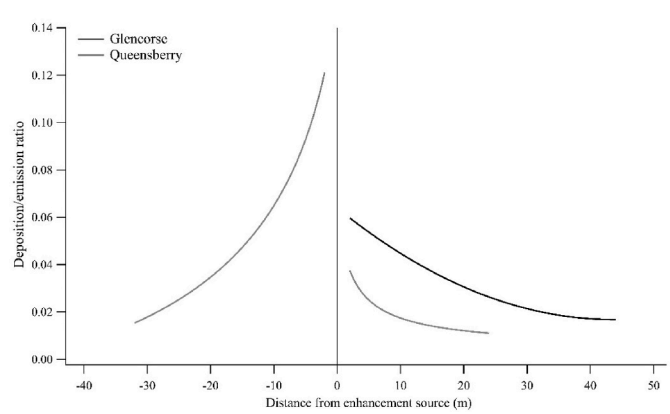

Fig. 19. Ratio of deposition to emission as a function of distance from the enhancement source at both sites.

forests. However, most studies estimate atmospheric NH_3 deposition from above canopy at background concentrations. It is rather difficult to compare our estimates with these studies because a) deposition occurs at our sites at enhanced concentrations, b) NH_3 is emitted from under the canopy, moving upwards, thereby not encountering above-canopy atmospheric resistance (R_a) and c) our canopy resistance (R_c) consists of a greater number of parallel resistances than most studies. It is therefore more useful to compare deposition velocities (V_d) rather than comparing the absolute deposition flux. We estimate mean V_d of 0.016 m s^{-1} (0.008–0.021 m s^{-1}) at Glencorse and 0.025 m s^{-1} (0.006–0.04 m s^{-1}) at Queensberry during the study period (see supplementary material for monthly values). Schrader et al. (2014) conducted a review of 42 studies estimating NH_3 V_d and calculated mean V_d of 0.015 m s^{-1} for mixed forests and 0.011 m s^{-1} for deciduous forests. To our knowledge, no study has reported V_d from a tropical forest. Inferential models estimate a wide range of NH_3 deposition velocities such as 0.008 m s^{-1} (CDRY), 0.011 m s^{-1} (EMEP-03), 0.022 m s^{-1} (IDEM), 0.024 m s^{-1} (CBED) (Flechard et al., 2011), 0.036 m s^{-1} (SCAIL) (Theobald et al., 2006) and 0.04 m s^{-1} (TERN + FRAME) (Dore et al., 2009; Singles et al., 1998) for forests. Few measured estimates of NH_3 deposition velocities for forests exist. Zhang et al. (2009) measured V_d over seven forested sites in Canada and estimated values of 0.0012–0.0063 m s^{-1}, much lower than other measured and modelled estimates. Other V_d estimates originate from measurements in coniferous forests such as Douglas Fir (0.02–0.032 m s^{-1}) (Duyzer et al., 1994; Wyers et al., 1992) and Spruce (0.009–0.04 m s^{-1}) (Andersen et al., 1999). Our values fall within the range of V_d estimated for forests from modelling and measurement studies. However, we provide the first V_d estimates for forests where R_a is not a contributing factor to the deposition process. Additionally, since in studies estimating atmospheric NH_3 deposition, R_c calculation often does not account for cuticular resistance and canopy compensation point, comparative estimates of deposition flux obtained with and without considering F_w and χ_c at both sites is provided (Table S5).

4. Conclusion

The enhancement system produced target NH_3 concentration and deposition levels along horizontal and vertical gradients downwind of the release. The system proved to be flexible for optimization and adaptation to contrasting forest types. The setup is being used to improve process-level understanding of physical aspects of dry deposition. This study presents a multi-layered resistance modelling approach that captures NH_3 exchange across canopy layers and helps identify the fate of excessive NH_3 within the forest canopy. It enables the partitioning of the deposition flux to understand which layers of the forest canopy are the largest NH_3 sinks and the dominant processes that drive deposition. At both our sites, with very different vegetation types, canopy structures and meteorological conditions, the soil surface and leaf cuticles of understorey vegetation emerged as the largest NH_3 sinks. In forest ecosystems that are located near NH_3 sources, the amount of NH_3 entering the canopy laterally is much larger than the NH_3 depositing from the atmosphere. In contrast to previous resistance models applied to forest canopies that are primarily concerned with atmospheric deposition, our model is applicable for identifying the fate of NH_3 in forest ecosystems where the gas enters the canopy laterally through the trunk space and exposes the understorey to high NH_3 levels. In the long term, along with NH_3 impacts on bark pH, tree growth and physiology, the potential for NH_3 recapture by forests will also be assessed. Experiments conducted at our sites will produce strong evidence of NH_3 impacts on sensitive and socio-economically important organisms such as lichen epiphytes, other aspects of biodiversity and ecosystem services. The findings will reinforce the need for effective policy changes to reduce NH_3 pollution. Our results show that trunk surfaces are the weakest NH_3 sinks out of all canopy layers. Despite this, lichens, which mainly occur on the tree trunks are known have severe impacts from NH_3 exposure. This highlights their value as bio-indicators with high sensitivity to NH_3 and further reinforces the importance of the NH_3 impact assessment studies established at both sites.

CRediT authorship contribution statement

Ajinkya G. Deshpande: Conceptualization, Data curation, Formal analysis, Investigation, Methodology, Resources, Software, Visualization, Writing – original draft. **Matthew R. Jones:** Conceptualization, Formal analysis, Investigation, Methodology, Resources, Supervision, Writing – review & editing. **Netty van Dijk:** Conceptualization, Data curation, Investigation, Methodology, Writing – review & editing. **Neil J. Mullinger:** Data curation, Investigation, Methodology, Resources, Software. **Duncan Harvey:** Investigation, Resources. **Robert Nicoll:** Resources, Software. **Galina Toteva:** Investigation, Resources. **Gothamie Weerakoon:** Investigation, Methodology, Supervision. **Sarath Nissanka:** Resources, Supervision. **Buddhika Weerakoon:** Data curation, Investigation, Resources. **Maude Grenier:** Investigation. **Agata Iwanicka:** Data curation, Investigation, Resources. **Fred Duarte:** Investigation. **Amy Stephens:** Data curation, Resources. **Christopher J. Ellis:** Conceptualization, Methodology, Writing – review & editing. **Massimo Vieno:** Conceptualization, Resources, Software. **Julia Drewer:** Investigation, Writing – review & editing. **Pat A. Wolseley:** Conceptualization. **Shamodi Nanayakkara:** Resources. **Tharindu Prabhashwara:** Resources. **William J. Bealey:** Project administration. **Eiko Nemitz:** Conceptualization, Formal analysis, Methodology, Resources, Supervision, Validation, Writing – review & editing. **Mark A. Sutton:** Conceptualization, Funding acquisition, Methodology, Resources, Supervision, Validation, Writing – review & editing.

Declaration of competing interest

The authors declare that they have no known competing financial interests or personal relationships that could have appeared to influence the work reported in this paper.

Data availability

Data will be made available on request.

Acknowledgement

The work was supported by UK Research and Innovation (UKRI) as a Global Challenges Research Fund grant, the 'GCRF South Asian Nitrogen Hub' (NE/S009019/1). It represents a contribution to the work of the GEF/UNEP International Nitrogen Management System (INMS) and the International Nitrogen Initiative (INI). The Glencorse field facility is also supported by the Natural Environment Research Council Award Number NE/R016429/1 as part of the UK-SCAPE programme delivering National Capability.

Appendix A. Supplementary data

Supplementary data to this article can be found online at https://doi.org/10.1016/j.atmosenv.2023.120325.

References

Andersen, H.V., Hovmand, M.F., Hummelshøj, P., Jensen, N.O., 1999. Measurements of ammonia concentrations, fluxes and dry deposition velocities to a spruce forest 1991–1995. Atmos. Environ. 33, 1367–1383. https://doi.org/10.1016/S1352-2310(98)00363-X.

Asman, W.A., 1998. Factors influencing local dry deposition of gases with special reference to ammonia. Atmos. Environ. 32, 415–421. https://doi.org/10.1016/S1352-2310(97)00166-0.

Baldocchi, D.D., Hicks, B.B., Camara, P., 1987. A canopy stomatal resistance model for gaseous deposition to vegetated surfaces. Atmos. Environ. 21, 91–101. https://doi.org/10.1016/0004-6981(87)90274-5, 1967.

Bealey, W.J., Loubet, B., Braban, C.F., Famulari, D., Theobald, M.R., Reis, S., Reay, D.S., Sutton, M.A., 2014. Modelling agro-forestry scenarios for ammonia abatement in the landscape. Environ. Res. Lett. 9, 125001 https://doi.org/10.1088/1748-9326/9/12/125001.

Bobbink, R., Loran, C., Tomassen, H., 2022. Review and Revision of Empirical Critical Loads of Nitrogen for Europe. German Environment Agency, Dessau, Germany.

Cape, J.N., Jones, M.R., Leith, I.D., Sheppard, L.J., van Dijk, N., Sutton, M.A., Fowler, D., 2008. Estimate of annual NH3 dry deposition to a fumigated ombrotrophic bog using concentration-dependent deposition velocities. Atmos. Environ. 42, 6637–6646. https://doi.org/10.1016/j.atmosenv.2008.04.027.

Cape, J.N., Tang, Y.S., van Dijk, N., Love, L., Sutton, M.A., Palmer, S.C.F., 2004. Concentrations of ammonia and nitrogen dioxide at roadside verges, and their contribution to nitrogen deposition. Environ. Pollut. 132, 469–478. https://doi.org/10.1016/j.envpol.2004.05.009.

Cape, J.N., van der Eerden, L.J., Sheppard, L.J., Leith, I.D., Sutton, M.A., 2009. Evidence for changing the critical level for ammonia. Environ. Pollut. 157, 1033–1037. https://doi.org/10.1016/j.envpol.2008.09.049.

Chamberlain, A.C., 1966. Transport of gases to and from grass and grass-like surfaces. Proc. Roy. Soc. Lond. A 290, 236–265. https://doi.org/10.1098/rspa.1966.0047.

Chamberlain, A.C., 1968. Transport of gases to and from surfaces with bluff and wave-like roughness elements. Q.J Royal Met. Soc. 94, 318–332. https://doi.org/10.1002/qj.49709440108.

Chamberlain, A.C., Garland, J.A., Wells, A.C., 1984. Transport of gases and particles to surfaces with widely spaced roughness elements. Boundary-Layer Meteorol. 29, 343–360. https://doi.org/10.1007/BF00120534.

Chatterjee, S., Bhattacharya, P., Kandya, A., 2017. A study on sustainable harvest of wild medicinal plants of Uttarakhand with a case study on lichens. Sustain For Emerg Challeng 163–193.

Clean Air Strategy, 2019. DEFRA [WWW Document]. URL. https://www.gov.uk/government/publications/clean-air-strategy-2019, 6.17.22.

David, M., Loubet, B., Cellier, P., Mattsson, M., Schjoerring, J.K., Nemitz, E., Roche, R., Riedo, M., Sutton, M.A., 2009. Ammonia sources and sinks in an intensively managed grassland canopy. Biogeosciences 6, 1903–1915. https://doi.org/10.5194/bg-6-1903-2009.

Dawson, G.A., 1977. Atmospheric ammonia from undisturbed land. J. Geophys. Res. 82, 3125–3133. https://doi.org/10.1029/JC082i021p03125.

Deshpande, A.G., 2020. Changing Hydroclimatic Conditions and Excessive Nitrogen Deposition Affect Ecosystem Functioning of a Bottomland Hardwood Forest (Doctoral Dissertation). Texas A&M University.

Dise, N.B., Ashmore, M., Belyazid, S., Bleeker, A., Bobbink, R., de Vries, W., Erisman, J. W., Spranger, T., Stevens, C.J., van den Berg, L., 2011. Nitrogen as a threat to European terrestrial biodiversity. In: Sutton, M.A., Howard, C.M., Erisman, J.W., Billen, G., Bleeker, A., Grennfelt, P., van Grinsven, H., Grizzetti, B. (Eds.), The European Nitrogen Assessment: Sources, Effects and Policy Perspectives. Cambridge University Press, pp. 463–494. https://doi.org/10.1017/CBO9780511976988.023.

Dore, A., Kryza, M., Hallsworth, S., Matejko, M., Hall, J., Van Oijen, M., Zhang, Y., Bealey, W.J., Vieno, M., Tang, Y.S., Smith, R., Dragosits, U., Sutton, M.A., 2009. Modelling the Deposition and Concentration of Long Range Air Pollutants: Final Report (No. CEH Project No: C03021). NERC/Centre for Ecology & Hydrology.

Duyzer, J.H., Verhagen, H.L.M., Weststrate, J.H., Bosveld, F.C., Vermetten, A.W.M., 1994. The dry deposition of ammonia onto a Douglas fir forest in The Netherlands. Atmos. Environ. 28, 1241–1253. https://doi.org/10.1016/1352-2310(94)90271-2.

EEA, 2016. European Union Emission Inventory Report 1990–2014 under the UNECE Convention on Long-Range Transboundary Air Pollution (LRTAP) (No. 16/2016). European Environment Agency.

Ellis, C.J., Steadman, C.E., Vieno, M., Chatterjee, S., Jones, M.R., Negi, S., Pandey, B.P., Rai, H., Tshering, D., Weerakoon, G., Wolseley, P., Reay, D., Sharma, S., Sutton, M., 2022. Estimating nitrogen risk to Himalayan forests using thresholds for lichen bioindicators. Biol. Conserv. 265, 109401 https://doi.org/10.1016/j.biocon.2021.109401.

Fagerli, H., Aas, W., 2008. Trends of nitrogen in air and precipitation: model results and observations at EMEP sites in Europe, 1980–2003. Environ. Pollut. 154, 448–461. https://doi.org/10.1016/j.envpol.2008.01.024.

Farquhar, G.D., Firth, P.M., Wetselaar, R., Weir, B., 1980. On the gaseous exchange of ammonia between leaves and the environment: determination of the ammonia compensation point. Plant Physiol 66, 710–714. https://doi.org/10.1104/pp.66.4.710.

Flechard, C.R., Fowler, D., Sutton, M.A., Cape, J.N., 1999. A dynamic chemical model of bi-directional ammonia exchange between semi-natural vegetation and the atmosphere. Q.J Royal Met. Soc. 125, 2611–2641. https://doi.org/10.1002/qj.49712555914.

Flechard, C.R., Nemitz, E., Smith, R.I., Fowler, D., Vermeulen, A.T., Bleeker, A., Erisman, J.W., Simpson, D., Zhang, L., Tang, Y.S., Sutton, M.A., 2011. Dry deposition of reactive nitrogen to European ecosystems: a comparison of inferential models across the NitroEurope network. Atmos. Chem. Phys. 11, 2703–2728. https://doi.org/10.5194/acp-11-2703-2011.

Flechard, C.R., Spirig, C., Neftel, A., Ammann, C., 2010. The annual ammonia budget of fertilised cut grassland – Part 2: seasonal variations and compensation point modeling. Biogeosciences 7, 537–556. https://doi.org/10.5194/bg-7-537-2010.

Forsmark, B., Wallander, H., Nordin, A., Gundale, M.J., 2021. Long-term nitrogen enrichment does not increase microbial phosphorus mobilization in a northern coniferous forest. Funct. Ecol. 35, 277–287. https://doi.org/10.1111/1365-2435.13701.

Fournier, N., Pais, V.A., Sutton, M.A., Weston, K.J., Dragosits, U., Tang, S.Y., Aherne, J., 2002. Parallelisation and application of a multi-layer atmospheric transport model to quantify dispersion and deposition of ammonia over the British Isles. Environ. Pollut. 116, 95–107. https://doi.org/10.1007/978-3-662-04956-3_1.

Fowler, D., 1978. Dry deposition of SO_2 on agricultural crops. Atmos. Environ. 12, 369–373. https://doi.org/10.1016/0004-6981(78)90219-6, 1967.

Fowler, D., Pitcairn, C.E.R., Sutton, M.A., Flechard, C., Loubet, B., Coyle, M., Munro, R. C., 1998. The mass budget of atmospheric ammonia in woodland within 1 km of livestock buildings. Environ. Pollut. 102, 343–348. https://doi.org/10.1016/S0269-7491(98)80053-5.

Fowler, D., Unsworth, M.H., 1979. Turbulent transfer of sulphur dioxide to a wheat crop. Q.J Royal Met. Soc. 105, 767–783. https://doi.org/10.1002/qj.49710544603.

Foyer, C.H., Parry, M., Noctor, G., 2003. Markers and signals associated with nitrogen assimilation in higher plants. J. Exp. Bot. 54, 585–593. https://doi.org/10.1093/jxb/erg053.

Franzaring, J., Jones, M.R., Kösler, J., Moravek, A., 2022. An overview of ammonia research. In: Franzaring, J., Kösler, J. (Eds.), Review of Internationally Proposed Critical Levels for Ammonia: Proceedings of an Expert Workshop Held in Dessau and Online on 28/29 March 2022. German Environment Agency, Dessau, Germany, pp. 11–31.

Franzaring, J., Kösler, J., 2022. Review of internationally proposed critical levels for ammonia. Proceedings of an Expert Workshop Held in Dessau and Online on 28/29 March 2022. German Environment Agency.

Garland, J.A., 1977. The dry deposition of sulphur dioxide to land and water surfaces. Proc. R. Soc. A 354, 245–268. https://doi.org/10.1098/rspa.1977.0066.

Ge, Y., Heal, M.R., Stevenson, D.S., Wind, P., Vieno, M., 2021. Evaluation of global EMEP MSC-W (rv4.34) WRF (v3.9.1.1)' ' model surface concentrations and wet deposition of reactive N and S with measurements. Geosci. Model Dev. (GMD) 14, 7021–7046. https://doi.org/10.5194/gmd-14-7021-2021.

Groot Koerkamp, P.W.G., Metz, J.H.M., Uenk, G.H., Phillips, V.R., Holden, M.R., Sneath, R.W., Short, J.L., White, R.P.P., Hartung, J., Seedorf, J., Schröder, M., Linkert, K.H., Pedersen, S., Takai, H., Johnsen, J.O., Wathes, C.M., 1998. Concentrations and emissions of ammonia in livestock buildings in northern europe. J. Agric. Eng. Res. 70, 79–95. https://doi.org/10.1006/jaer.1998.0275.

Gundale, M.J., Deluca, T.H., Nordin, A., 2011. Bryophytes attenuate anthropogenic nitrogen inputs in boreal forests. Glob. Change Biol. 17, 2743–2753. https://doi.org/10.1111/j.1365-2486.2011.02407.x.

Gurmesa, G.A., Wang, A., Li, S., Peng, S., de Vries, W., Gundersen, P., Ciais, P., Phillips, O.L., Hobbie, E.A., Zhu, W., Nadelhoffer, K., Xi, Y., Bai, E., Sun, T., Chen, D., Zhou, W., Zhang, Y., Guo, Y., Zhu, J., Duan, L., Li, D., Koba, K., Du, E., Zhou, G., Han, X., Han, S., Fang, Y., 2022. Retention of deposited ammonium and nitrate and its impact on the global forest carbon sink. Nat. Commun. 13, 880. https://doi.org/10.1038/s41467-022-28345-1.

Hansen, K., Personne, E., Skjøth, C.A., Loubet, B., Ibrom, A., Jensen, R., Sørensen, L.L., Boegh, E., 2017. Investigating sources of measured forest-atmosphere ammonia fluxes using two-layer bi-directional modelling. Agric. For. Meteorol. 237–238, 80–94. https://doi.org/10.1016/j.agrformet.2017.02.008.

Hao, X., Chang, C., Janzen, H.H., Clayton, G., Hill, B.R., 2006. Sorption of atmospheric ammonia by soil and perennial grass downwind from two large cattle feedlots. J. Environ. Qual. 35, 1960–1965. https://doi.org/10.2134/jeq2005.0308.

Hartmann, A., 2005. Erarbeitung von Methoden zur Extraktion der Extrazellularflussigkeit von Fichtennadeln Fur die Bestimmungdes Ammoniak-Kompensationspunktes. Interdisziplinäres Okologisches Zentrum (Bergakademie Freiberg).

He, X., Hou, E., Veen, G.F., Ellwood, M.D.F., Dijkstra, P., Sui, X., Zhang, S., Wen, D., Chu, C., 2020. Soil microbial biomass increases along elevational gradients in the tropics and subtropics but not elsewhere. Global Ecol. Biogeogr. 29, 345–354. https://doi.org/10.1111/geb.13017.

Hicks, B.B., Baldocchi, D.D., Meyers, T.P., Hosker, R.P., Matt, D.R., 1987. A preliminary multiple resistance routine for deriving dry deposition velocities from measured quantities. Water. Air. Soil Pollut. 36, 311–330. https://doi.org/10.1007/BF00229675.

Hill, P.W., Raven, J.A., Sutton, M.A., 2002. Leaf age-related differences in apoplastic NH(4)(+) concentration, pH and the NH(3) compensation point for a wild perennial. J. Exp. Bot. 53, 277–286. https://doi.org/10.1093/jexbot/53.367.277.

Husted, S., Schjoerring, J.K., 1995. Apoplastic pH and ammonium concentration in leaves of Brassica napus L. Plant Physiol 109, 1453–1460. https://doi.org/10.1104/pp.109.4.1453.

Jarvis, P.G., 1976. The interpretation of the variations in leaf water potential and stomatal conductance found in canopies in the field. Philos. Trans. R. Soc. Lond. B Biol. Sci. 273, 593–610. https://doi.org/10.1098/rstb.1976.0035.

Jones, M.R., Leith, I.D., Fowler, D., Raven, J.A., Sutton, M.A., Nemitz, E., Cape, J.N., Sheppard, L.J., Smith, R.I., Theobald, M.R., 2007a. Concentration-dependent NH3 deposition processes for mixed moorland semi-natural vegetation. Atmos. Environ. 41, 2049–2060. https://doi.org/10.1016/j.atmosenv.2006.11.003.

Jones, M.R., Leith, I.D., Raven, J.A., Fowler, D., Sutton, M.A., Nemitz, E., Cape, J.N., Sheppard, L.J., Smith, R.I., 2007b. Concentration-dependent NH3 deposition processes for moorland plant species with and without stomata. Atmos. Environ. 41, 8980–8994. https://doi.org/10.1016/j.atmosenv.2007.08.015.

Kamp, J.N., Häni, C., Nyord, T., Feilberg, A., Sørensen, L.L., 2020. The aerodynamic gradient method: implications of non-simultaneous measurements at alternating heights. Atmosphere 11, 1067. https://doi.org/10.3390/atmos11101067.

Kesselmeier, J., Merk, L., Bliefernicht, M., Helas, G., 1993. Trace gas exchange between terrestrial plants and atmosphere: carbon dioxide, carbonyl sulfide and ammonia under the rule of compensation points. In: General Assessment of Biogenic Emissions and Deposition of Nitrogen Compounds, Sulphur Compounds and Oxidants in Europe. Brussels, pp. 71–80.

Kruit, R.J.W., van Pul, W.A.J., Sauter, F.J., van den Broek, M., Nemitz, E., Sutton, M.A., Krol, M., Holtslag, A.A.M., 2010. Modeling the surface–atmosphere exchange of ammonia. Atmos. Environ. 44, 945–957. https://doi.org/10.1016/j.atmosenv.2009.11.049.

Lalic, B., Mihailovic, D.T., Rajkovic, B., Arsenic, I.D., Radlovic, D., 2003. Wind profile within the forest canopy and in the transition layer above it. Environ. Model. Software 18, 943–950. https://doi.org/10.1016/S1364-8152(03)00068-9.

Langford, A.O., Fehsenfeld, F.C., 1992. Natural vegetation as a source or sink for atmospheric ammonia: a case study. Science 255, 581–583. https://doi.org/10.1126/science.255.5044.581.

Langford, A.O., Fehsenfeld, F.C., Zachariassen, J., Schimel, D.S., 1992. Gaseous ammonia fluxes and background concentrations in terrestrial ecosystems of the United States. Global Biogeochem. Cycles 6, 459–483. https://doi.org/10.1029/92GB02123.

Leegood, R.C., Lea, P.J., Adcock, M.D., Häusler, R.E., 1995. The regulation and control of photorespiration. J. Exp. Bot. 46, 1397–1414. https://doi.org/10.1093/jxb/46.special_issue.1397.

Leeson, S.R., Levy, P.E., van Dijk, N., Drewer, J., Robinson, S., Jones, M.R., Kentisbeer, J., Washbourne, I., Sutton, M.A., Sheppard, L.J., 2017. Nitrous oxide emissions from a peatbog after 13 years of experimental nitrogen deposition. Biogeosciences 14, 5753–5764. https://doi.org/10.5194/bg-14-5753-2017.

Leith, I.D., Sheppard, L.J., Fowler, D., Cape, J.N., Jones, M., Crossley, A., Hargreaves, K. J., Tang, Y.S., Theobald, M., Sutton, M.R., 2004. Quantifying dry NH3 deposition to an ombrotrophic bog from an automated NH3 field release system. Water Air Soil Pollut. Focus 4, 207–218. https://doi.org/10.1007/s11267-005-3031-y.

Li, J., Yang, L., Li, X., Zheng, H., 2016. Visualization of local wind field based forest-fire's forecast modeling for transportation planning. Multimed. Tool. Appl. 1–15. https://doi.org/10.1007/s11042-016-3357-7.

Loubet, B., Milford, C., Hill, P.W., Sim Tang, Y., Cellier, P., Sutton, M.A., 2002. Seasonal variability of apoplastic NH4 + and pH in an intensively managed grassland. Plant Soil.

Ma, X., Wang, T., Shi, Z., Chiariello, N.R., Docherty, K., Field, C.B., Gutknecht, J., Gao, Q., Gu, Y., Guo, X., Hungate, B.A., Lei, J., Niboyet, A., Le Roux, X., Yuan, M., Yuan, T., Zhou, J., Yang, Y., 2022. Long-term nitrogen deposition enhances microbial capacities in soil carbon stabilization but reduces network complexity. Microbiome 10, 112. https://doi.org/10.1186/s40168-022-01309-9.

Manninen, S., Jääskeläinen, K., Stephens, A., Iwanicka, A., Tang, S., van Dijk, N., 2023. NH3 concentrations below the current critical level affect the epiphytic macrolichen communities - evidence from a Northern European City. Sci. Total Environ. 877, 162877 https://doi.org/10.1016/j.scitotenv.2023.162877.

Martin, N.A., Ferracci, V., Cassidy, N., Hoffnagle, J.A., 2016. The application of a cavity ring-down spectrometer to measurements of ambient ammonia using traceable primary standard gas mixtures. Appl. Phys. B 122, 219. https://doi.org/10.1007/s00340-016-6486-9.

Massad, R.S., Nemitz, E., Sutton, M.A., 2010. Review and parameterisation of bi-directional ammonia exchange between vegetation and the atmosphere. Atmos. Chem. Phys. 10, 10359–10386. https://doi.org/10.5194/acp-10-10359-2010.

Mattsson, M., Herrmann, B., David, M., Loubet, B., Riedo, M., Theobald, M.R., Sutton, M. A., Bruhn, D., Neftel, A., Schjoerring, J.K., 2009. Temporal variability in bioassays of the stomatal ammonia compensation point in relation to plant and soil nitrogen parameters in intensively managed grassland. Biogeosciences 6, 171–179. https://doi.org/10.5194/bg-6-171-2009.

Mattsson, M., Schjoerring, J.K., 1996. Ammonia emission from young barley plants: influence of N source, light/dark cycles and inhibition of glutamine synthetase. J. Exp. Bot. 47, 477–484. https://doi.org/10.1093/jxb/47.4.477.

Meyers, T.P., Finkelstein, P., Clarke, J., Ellestad, T.G., Sims, P.F., 1998. A multilayer model for inferring dry deposition using standard meteorological measurements. J. Geophys. Res. 103, 22645–22661. https://doi.org/10.1029/98JD01564.

Moon, K., Duff, T.J., Tolhurst, K.G., 2013. Characterising forest wind profiles for utilisation in firespread models. In: Piantadosi, J., Anderssen, R.S., Boland, J. (Eds.), Presented at the 20th International Congress on Modelling and Simulation, Modelling and Simulation Society of Australia and New Zealand, Adelaide, Australia, pp. 214–220.

Moon, K., Duff, T.J., Tolhurst, K.G., 2016. Sub-canopy forest winds: understanding wind profiles for fire behaviour simulation. Fire Saf. J. https://doi.org/10.1016/j.firesaf.2016.02.005.

Murphy, C.E., Sigmon, J.T., 1990. Dry deposition of sulfur and nitrogen oxide gases to forest vegetation. In: Lindberg, S.E., Page, A.L., Norton, S.A. (Eds.), Acidic Precipitation: Sources, Deposition, and Canopy Interactions, Advances in Environmental Science. Springer New York, New York, NY, pp. 217–240. https://doi.org/10.1007/978-1-4612-4454-7_6.

Neill, C., Piccolo, M.C., Melillo, J.M., Steudler, P.A., Cerri, C.C., 1999. Nitrogen dynamics in Amazon forest and pasture soils measured by 15N pool dilution. Soil Biol. Biochem. 31, 567–572. https://doi.org/10.1016/S0038-0717(98)00159-X.

Neirynck, J., Ceulemans, R., 2008. Bidirectional ammonia exchange above a mixed coniferous forest. Environ. Pollut. 154, 424–438. https://doi.org/10.1016/j.envpol.2007.11.030.

Nemitz, E., Milford, C., Sutton, M.A., 2001. A two-layer canopy compensation point model for describing bi-directional biosphere-atmosphere exchange of ammonia. Q.J Royal Met. Soc. 127, 815–833. https://doi.org/10.1002/qj.49712757306.

Nemitz, E., Sutton, M.A., Gut, A., San José, R., Husted, S., Schjoerring, J.K., 2000a. Sources and sinks of ammonia within an oilseed rape canopy. Agric. For. Meteorol. 105, 385–404. https://doi.org/10.1016/S0168-1923(00)00205-7.

Nemitz, E., Sutton, M.A., Schjoerring, J.K., Husted, S., Paul Wyers, G., 2000b. Resistance modelling of ammonia exchange over oilseed rape. Agric. For. Meteorol. 105, 405–425. https://doi.org/10.1016/S0168-1923(00)00206-9.

Nemitz, E., Sutton, M.A., Wyers, G.P., Jongejan, P.A.C., 2004. Gas-particle interactions above a Dutch heathland: I. Surface exchange fluxes of NH_3, SO_2, HNO_3 and HCl. Atmos. Chem. Phys. 4, 989–1005. https://doi.org/10.5194/acp-4-989-2004.

Nielsen, K.H., Schjoerring, J.K., 1998. Regulation of apoplastic NH_4^+ concentration in leaves of oilseed rape. Plant Physiol 118, 1361–1368. https://doi.org/10.1104/pp.118.4.1361.

Oliver, H.R., 1971. Wind profiles in and above a forest canopy. Q.J Royal Met. Soc. 97, 548–553. https://doi.org/10.1002/qj.49709741414.

Owen, P.R., Thomson, W.R., 1963. Heat transfer across rough surfaces. J. Fluid Mech. 15, 321–334. https://doi.org/10.1017/S0022112063000288.

Parton, W.J., Morgan, J.A., Altenhofen, J.M., Harper, L.A., 1988. Ammonia volatilization from spring wheat plants. Agron. J. 80, 419–425. https://doi.org/10.2134/agronj1988.00021962008000030008x.

Pearson, J., Clough, E.C.M., Woodall, J., Havill, D.C., Zhang, X.H., 1998. Ammonia emissions to the atmosphere from leaves of wild plants and *Hordeum vulgare* treated with methionine sulphoximine. New Phytol. 138, 37–48. https://doi.org/10.1046/j.1469-8137.1998.00880.x.

Pitcairn, C.E.R., Leith, I.D., Sheppard, L.J., Sutton, M.A., Fowler, D., Munro, R.C., Tang, S., Wilson, D., 1998. The relationship between nitrogen deposition, species composition and foliar nitrogen concentrations in woodland flora in the vicinity of livestock farms. Environ. Pollut. 102, 41–48. https://doi.org/10.1016/S0269-7491(98)80013-4.

Posthumus, A.C., 1988. Critical levels for effects of ammonia and ammonium. Presented at the Procedings of the Bad Harzburg Workshop. UBA, Berlin, pp. 117–127.

Ramsay, R., Di Marco, C.F., Heal, M.R., Sörgel, M., Artaxo, P., Andreae, M.O., Nemitz, E., 2021. Measurement and modelling of the dynamics of NH_3 surface–atmosphere exchange over the Amazonian rainforest. Biogeosciences 18, 2809–2825. https://doi.org/10.5194/bg-18-2809-2021.

Rowe, E., Hina, N., Carnell, E., Vieno, M., Levy, P., Raine, B., Sawicka, K., Tomlinson, S., Hernandez, C.M., Jones, L., 2022. Trends Report 2022: Trends in Critical Load and Critical Level Exceedances in the UK, Report to Defra under Contract AQ0849,' ' CEH Project 07617. DEFRA.

Santana, R.A.S. de, Dias-Júnior, C.Q., Vale, R.S. do, Tóta, J., Fitzjarrald, D.R., 2017. Observing and modeling the vertical wind profile at multiple sites in and above the amazon rain forest canopy. Adv. Meteorol. 1–8. https://doi.org/10.1155/2017/5436157, 2017.

Schjoerring, J.K., Husted, S., Mäck, G., Mattsson, M., 2002. The regulation of ammonium translocation in plants. J. Exp. Bot. 53, 883–890. https://doi.org/10.1093/jexbot/53.370.883.

Schrader, F., Brümmer, C., 2014. Land use specific ammonia deposition velocities: a review of recent studies (2004-2013). Water. Air. Soil Pollut. 225, 2114. https://doi.org/10.1007/s11270-014-2114-7.

Schuepp, P.H., 1977. Turbulent transfer at the ground: on verification of a simple predictive model. Boundary-Layer Meteorol. 12, 171–186. https://doi.org/10.1007/BF00121971.

Shaw, R.H., 1977. Secondary wind speed maxima inside plant canopies. J. Appl. Meteorol. 16, 514–521. https://doi.org/10.1175/1520-0450(1977)016<0514:SWSMIP>2.0.CO;2.

Shen, J., Chen, D., Bai, M., Sun, J., Lam, S.K., Mosier, A., Liu, X., Li, Y., 2018. Spatial variations in soil and plant nitrogen levels caused by ammonia deposition near a cattle feedlot. Atmos. Environ. 176, 120–127. https://doi.org/10.1016/j.atmosenv.2017.12.022.

Sheppard, L.J., Leith, I.D., Mizunuma, T., Neil Cape, J., Crossley, A., Leeson, S., Sutton, M.A., Dijk, N., Fowler, D., 2011. Dry deposition of ammonia gas drives species change faster than wet deposition of ammonium ions: evidence from a long-term field manipulation. Glob. Change Biol. 17, 3589–3607. https://doi.org/10.1111/j.1365-2486.2011.02478.x.

Silver, W.L., Herman, D.J., Firestone, M.K., 2001. Dissimilatory nitrate reduction to ammonium in upland tropical forest soils. Ecology 82, 2410. https://doi.org/10.2307/2679925.

Simpson, D., Benedictow, A., Berge, H., Bergström, R., Emberson, L.D., Fagerli, H., Flechard, C.R., Hayman, G.D., Gauss, M., Jonson, J.E., Jenkin, M.E., Nyíri, A., Richter, C., Semeena, V.S., Tsyro, S., Tuovinen, J.P., Valdebenito, Á., Wind, P., 2012. The EMEP MSC-W chemical transport model – technical description. Atmos. Chem. Phys. 12, 7825–7865. https://doi.org/10.5194/acp-12-7825-2012.

Singles, R., Sutton, M.A., Weston, K.J., 1998. A multi-layer model to describe the atmospheric transport and deposition of ammonia in Great Britain. Atmos. Environ. 32, 393–399. https://doi.org/10.1016/S1352-2310(97)83467-X.

Subhasinghe, S.A.P., 1988. Soil Map of Sri Lanka. Land Use Division, Irrigation Department, Govt. of Sri Lanka, Colombo.

Sutton, M., 2007. Report of Site Visit 16 January 2007 to Moninea Bog, Special Area of Conservation, Northern Ireland, Including Results from Foliar Bioassay Determinations and Subsequent Ammonia Monitoring. Centre for Ecology and Hydrology, Edinburgh, Scotland.

Sutton, M., Fowler, D., 1993. A model for inferring bi-directional fluxes of ammonia over plant canopies. Presented at the Proceedings of the WMO Conference on the Measurement and Modelling of Atmospheric Composition Changes Including Pollution Transport. WMO, Sofia, Bulgaria, pp. 179–182.

Sutton, M.A., Asman, W.A.H., Ellermann, T., Van Jaarsveld, J.A., Acker, K., Aneja, V., Duyzer, J., Horvath, L., Paramonov, S., Mitosinkova, M., Tang, Y.S., Achermann, B., Gauger, T., Bartniki, J., Neftel, A., Erisman, J.W., 2003. Establishing the link between ammonia emission control and measurements of reduced nitrogen concentrations and deposition. Environ. Monit. Assess. 82, 149–185. https://doi.org/10.1023/a:1021834132138.

Sutton, M.A., Asman, W.A.H., Schjorring, J.K., 1994. Dry deposition of reduced nitrogen. Tellus B 46, 255–273. https://doi.org/10.1034/j.1600-0889.1994.t01-2-00002.x.

Sutton, M.A., Burkhardt, J.K., Guerin, D., Fowler, D., 1995a. Measurement and modelling of ammonia exchange over arable croplands. In: Acid Rain Research: Do We Have Enough Answers?, Proceedings of a Specialty Conference, Studies in Environmental Science. Elsevier, pp. 71–80. https://doi.org/10.1016/S0166-1116(06)80274-8.

Sutton, M.A., Burkhardt, J.K., Guerin, D., Nemitz, E., Fowler, D., 1998a. Development of resistance models to describe measurements of bi-directional ammonia surface–atmosphere exchange. Atmos. Environ. 32, 473–480. https://doi.org/10.1016/S1352-2310(97)00164-7.

Sutton, M.A., Flower, D., Moncriefe, J.B., 1993a. The exchange of atmospheric ammonia with vegetated surfaces. I: unfertilized vegetation. Q.J Royal Met. Soc 119, 1023–1045. https://doi.org/10.1002/qj.49711951309.

Sutton, M.A., Fowler, D., Moncrieft, J.B., Storeton-West, R.L., 1993b. The exchange of atmospheric ammonia with vegetated surfaces. II: fertilized vegetation. Q.J Royal Met. Soc. 119, 1047–1070. https://doi.org/10.1002/qj.49711951310.

Sutton, M.A., Howard, C.M., 2018. Satellite pinpoints ammonia sources globally. Nature 564, 49–50. https://doi.org/10.1038/d41586-018-07584-7.

Sutton, M.A., Leith, I.D., Wj, B., van Dijk, N., Tang, Y.S., 2011. Moninea Bog - Case Study of Atmospheric Ammonia Impacts on a Special Area of Conservation (No. COST729), Nitrogen Deposition and Natura 2000: Science and Practice in DeterminingEnvironmental Impacts. COST.

Sutton, M.A., Milford, C., Dragosits, U., Place, C.J., Singles, R.J., Smith, R.I., Pitcairn, C. E.R., Fowler, D., Hill, J., ApSimon, H.M., Ross, C., Hill, R., Jarvis, S.C., Pain, B.F., Phillips, V.C., Harrison, R., Moss, D., Webb, J., Espenhahn, S.E., Lee, D.S., Hornung, M., Ullyett, J., Bull, K.R., Emmett, B.A., Lowe, J., Wyers, G.P., 1998b. Dispersion, deposition and impacts of atmospheric ammonia: quantifying local budgets and spatial variability. Environ. Pollut. 102, 349–361. https://doi.org/10.1016/S0269-7491(98)80054-7.

Sutton, M.A., Moncrieff, J.B., Fowler, D., 1992. Deposition of atmospheric ammonia to moorlands. Environ. Pollut. 75, 15–24. https://doi.org/10.1016/0269-7491(92)90051-B.

Sutton, M.A., Nemitz, E., Milford, C., Campbell, C., Erisman, J.W., Hensen, A., Cellier, P., David, M., Loubet, B., Personne, E., Schjoerring, J.K., Mattsson, M., Dorsey, J.R., Gallagher, M.W., Horvath, L., Weidinger, T., Meszaros, R., Dämmgen, U., Neftel, A., Herrmann, B., Lehman, B.E., Flechard, C., Burkhardt, J., 2009a. Dynamics of ammonia exchange with cut grassland: synthesis of results and conclusions of the GRAMINAE Integrated Experiment. Biogeosciences 6, 2907–2934. https://doi.org/10.5194/bg-6-2907-2009.

Sutton, M.A., Reis, S., Baker, S.M.H., 2009b. Atmospheric Ammonia. Springer, Dordrecht.

Sutton, M.A., Schjorring, J.K., Wyers, G.P., Duyzer, J.H., Ineson, P., Powlson, D.S., 1995b. Plant-atmosphere exchange of ammonia [and discussion]. Phil. Trans. Phys. Sci. Eng. 351, 261.

Sutton, M.A., van Dijk, N., Levy, P.E., Jones, M.R., Leith, I.D., Sheppard, L.J., Leeson, S., Sim Tang, Y., Stephens, A., Braban, C.F., Dragosits, U., Howard, C.M., Vieno, M., Fowler, D., Corbett, P., Naikoo, M.I., Munzi, S., Ellis, C.J., Chatterjee, S., Steadman, C.E., Móring, A., Wolseley, P.A., 2020. Alkaline air: changing perspectives on nitrogen and air pollution in an ammonia-rich world. Philos. Trans. A, Math. Phys. Eng. Sci. 378, 20190315 https://doi.org/10.1098/rsta.2019.0315.

Sutton, M.A., Wolseley, P.A., van Dijk, N., Deshpande, A.G., Dragosits, U., Twigg, M.M., Tang, Y.S., Braban, C.F., Levy, P., Bealey, W.J., Weerakoon, G., Jiang, J., Stevenson, D.S., Weerakoon, B., Nissanka, S.P., Jones, M.R., 2022. 15 years on: rationale and reflection on the 2006 Edinburgh Ammonia Workshop in the light of emerging evidence. In: Franzaring, J., Kösler, J. (Eds.), Proceedings of an Expert Workshop Held in Dessau and Online on 28/29 March 2022. Presented at the Review of Internationally Proposed Critical Levels for Ammonia. Umweltbundesamt, Dessau, Germany, pp. 36–46.

Tang, Y.S., Braban, C.F., Dragosits, U., Dore, A.J., Simmons, I., van Dijk, N., Poskitt, J., Dos Santos Pereira, G., Keenan, P.O., Conolly, C., Vincent, K., Smith, R.I., Heal, M.R., Sutton, M.A., 2018. Drivers for spatial, temporal and long-term trends in atmospheric ammonia and ammonium in the UK. Atmos. Chem. Phys. 18, 705–733. https://doi.org/10.5194/acp-18-705-2018.

Tang, Y.S., Cape, J.N., Sutton, M.A., 2001. Development and types of passive samplers for monitoring atmospheric NO2 and NH3 concentrations. Sci. World J. 1, 513–529. https://doi.org/10.1100/tsw.2001.82.

Tanner, E., Buchmann, N., Eugster, W., 2022. Agricultural ammonia dry deposition and total nitrogen deposition to a Swiss mire. Agric. Ecosyst. Environ. 336, 108009 https://doi.org/10.1016/j.agee.2022.108009.

Theobald, M.R., Bealey, W.J., Sutton, M.A., 2006. Refining the Simple Calculation of Ammonia Impact Limits (SCAIL) Model for Application in Scotland (No. AS 06/09). Centre for Ecology and Hydrology, Edinburgh.

Theobald, M.R., Milford, C., Hargreaves, K.J., Sheppard, L.J., Nemitz, E., Tang, Y.S., Phillips, V.R., Sneath, R., McCartney, L., Harvey, F.J., Leith, I.D., Cape, J.N., Fowler, D., Sutton, M.A., 2001. Potential for ammonia recapture by farm woodlands: design and application of a new experimental facility. Sci. World J. 1 (Suppl. 2), 791–801. https://doi.org/10.1100/tsw.2001.338.

Thom, A.S., 1975. Momentum, mass and heat exchange of plant communities. In: Monteith, J.L. (Ed.), Vegetation and the Atmosphere. Academic Press, London, pp. 57–109.

UNECE, 2007. Report on the Workshop on Atmospheric Ammonia: Detecting Emission Changes and Environmental Impacts. No. ECE/ED.AIR/WG.5/2007/3). Geneva United Nations Economic and Social Council (UNECE), Executive body for the Convention of Long-Range Transboundary Air pollution: Working Group on Strategies and Review.

Van Damme, M., Clarisse, L., Whitburn, S., Hadji-Lazaro, J., Hurtmans, D., Clerbaux, C., Coheur, P.-F., 2018. Industrial and agricultural ammonia point sources exposed. Nature 564, 99–103. https://doi.org/10.1038/s41586-018-0747-1.

van Herk, C.M., 2001. Bark pH and susceptibility to toxic air pollutants as independent causes of changes in epiphytic lichen composition in space and time. LIC 33, 419–442. https://doi.org/10.1006/lich.2001.0337.

van Zanten, M.C., Sauter, F.J., Wichink Kruit, R.J., van Jaarsveld, J.A., van Pul, W.A.J., 2010. Description of the DEPAC Module (No. RIVM Report 680180001/2010). National Institute for Public Health and the Environment RIVM, The Netherlands.

Vieno, M., Dore, A.J., Wind, P., Marco, C.D., Nemitz, E., Phillips, G., Tarrasón, L., Sutton, M.A., 2009. Application of the EMEP unified model to the UK with a horizontal resolution of 5 × 5 km2. In: Sutton, M.A., Reis, S., Baker, S.M.H. (Eds.), Atmospheric Ammonia. Springer Netherlands, Dordrecht, pp. 367–372. https://doi.org/10.1007/978-1-4020-9121-6_21.

Vieno, M., Heal, M.R., Williams, M.L., Carnell, E.J., Nemitz, E., Stedman, J.R., Reis, S., 2016. The sensitivities of emissions reductions for the mitigation of UK $PM_{2.5}$. Atmos. Chem. Phys. 16, 265–276. https://doi.org/10.5194/acp-16-265-2016.

Walker, J., Spence, P., Kimbrough, S., Robarge, W., 2008. Inferential model estimates of ammonia dry deposition in the vicinity of a swine production facility. Atmos. Environ. 42, 3407–3418. https://doi.org/10.1016/j.atmosenv.2007.06.004.

Wang, L., Xu, Y., Schjoerring, J.K., 2011. Seasonal variation in ammonia compensation point and nitrogen pools in beech leaves (Fagus sylvatica). Plant Soil 343, 51–66. https://doi.org/10.1007/s11104-010-0693-7.

Weerakoon, G., Aptroot, A., 2014. Over 200 new lichen records from Sri Lanka, with three new species to science. Cryptog. Mycolog. 35, 51–62. https://doi.org/10.7872/crym.v35.iss1.2014.51.

Wesely, M.L., Cook, D.R., Hart, R.L., Speer, R.E., 1985. Measurements and parameterization of particulate sulfur dry deposition over grass. J. Geophys. Res. 90, 2131. https://doi.org/10.1029/JD090iD01p02131.

Wesely, M.L., Hicks, B.B., 1977. Some factors that affect the deposition rates of sulfur dioxide and similar gases on vegetation. J. Air Pollut. Control Assoc. 27, 1110–1116. https://doi.org/10.1080/00022470.1977.10470534.

Wolseley, P.A., James, P.W., Theobald, M.R., Sutton, M.A., 2006. Detecting changes in epiphytic lichen communities at sites affected by atmospheric ammonia from agricultural sources. LIC 38, 161–176. https://doi.org/10.1017/S0024282905005487.

Wyers, G., Erisman, J.W., 1998. Ammonia exchange over coniferous forest. Atmos. Environ. 32, 441–451. https://doi.org/10.1016/S1352-2310(97)00275-6.

Wyers, G.P., Vermeulen, A.T., Slanina, J., 1992. Measurement of dry deposition of ammonia on a forest. Environ. Pollut. 75, 25–28. https://doi.org/10.1016/0269-7491(92)90052-c.

Xu, X., Thornton, P.E., Post, W.M., 2013. A global analysis of soil microbial biomass carbon, nitrogen and phosphorus in terrestrial ecosystems. Global Ecol. Biogeogr. 22, 737–749. https://doi.org/10.1111/geb.12029.

Yi, W., Shen, J., Liu, G., Wang, J., Yu, L., Li, Y., Reis, S., Wu, J., 2021. High NH_3 deposition in the environs of a commercial fattening pig farm in central south China. Environ. Res. Lett. 16, 125007 https://doi.org/10.1088/1748-9326/ac3603.

Yi, Y., Shen, J., Yang, C., Wang, J., Li, Y., Wu, J., 2020. Dry deposition of ammonia around paddy fields in the subtropical hilly area in southern China. Atmospheric and Oceanic Science Letters 13, 216–223. https://doi.org/10.1080/16742834.2020.1738208.

Zeng, P., Takahashi, H., 2000. A first-order closure model for the wind flow within and above vegetation canopies. Agric. For. Meteorol. 103, 301–313. https://doi.org/10.1016/S0168-1923(00)00133-7.

Zhang, L., Brook, J.R., Vet, R., 2003. A revised parameterization for gaseous dry deposition in air-quality models. Atmos. Chem. Phys. 3, 2067–2082. https://doi.org/10.5194/acp-3-2067-2003.

Zhang, L., Vet, R., O'Brien, J.M., Mihele, C., Liang, Z., Wiebe, A., 2009. Dry deposition of individual nitrogen species at eight Canadian rural sites. J. Geophys. Res. 114 https://doi.org/10.1029/2008JD010640.